

AN OPTICAL STUDY OF THE FAINT END OF THE STELLAR LUMINOSITY FUNCTION

William Jarrett^{1,2},

R.L. Dickman^{1,3}

and

w. Herbst⁴

Received

¹ Department of Physics and Astronomy, University of Massachusetts, Amherst.

² NRC Resident Research Associate, Infrared Processing and Analysis Center, California Institute of Technology, Jet Propulsion Laboratory, 4800 G St., Pasadena, CA 91125.

³ Division of Astronomical Sciences, National Science Foundation, 1800 G St. N. W., Washington, D.C. 20550.

⁴ Van Vleck Observatory, Wesleyan University, Middletown, CT 06457.

ABSTRACT

We implement a new method by which to study the faint end of the field star luminosity function. The method relies on deep, multicolor photometry of fields projected against highly obscured, nearby molecular clouds. The clouds act as nearly opaque screens and delimit a well-defined survey volume which is in principle free of the problem of distinguishing nearby, intrinsically faint dwarf stars from more distant red giants.

This study is based upon deep photographic and CCD photometry at optical (V, R, I) bandpasses towards the most highly obscured portions of the Taurus and Ophiuchus molecular clouds. The total volume delimited by the clouds is $\sim 200''$ pc³. Within this region our survey is complete for all stars brighter than $M_v = 16-17$ mag; at R and I, the survey is complete down to the lowest mass stars capable of sustaining core hydrogen burning.

Color-color criteria are used to distinguish between background, highly reddened stars and stars located in front of the clouds, and the method of photometric parallax is used to deduce the absolute magnitudes and spectral types of those stars found to lie in front of the clouds. To help further resolve foreground/background ambiguities we have made proper motion measurements of the candidate foreground stars using the photographic and CCD data, and the Palomar Sky Survey.

We estimate the faint end of the field star luminosity function for the composite Taurus and Ophiuchus foreground sample and find that it resembles the *local* luminosity function down to $M_v = 16$. At still fainter magnitudes we find more stars than do photometric parallax studies of the polar regions. This difference widens dramatically if even the simplest correction for incompleteness is applied to our data. We therefore tentatively conclude that the luminosity function rises beyond $M_v = 1$ (i; even if we discard our attempts to correct for incompleteness in the faintest magnitude bins, the luminosity function at least remains flat for the lowest mass stars.

Our provisional finding that the luminosity function rises again beyond its well-known peak at $M_v \sim 12-13$, implies that the IMF probably rises beyond the turnover point associated with this peak. Even if our most conservative estimate for the faint end of the luminosity function is used - in which no corrections are made for incompleteness - the IMF must at least remain flat down to the edge of the hydrogen-burning main sequence.

Subject Headings: Stars: Late-Type, Low-Mass; Photometry; Luminosity Function; Astrometry.

1. Introduction

Notwithstanding its basic importance, the initial mass function (IMF; Salpeter 1955) is poorly known in a number of ways, and as Scalo (1986) has emphasized, the very existence of a widely applicable mass function remains more assumption than observationally established fact. While the general hope is that the physics of star formation is sufficiently universal to promote the existence of a mass distribution which varies only gently with the various factors known to influence star formation (such as metallicity and molecular cloud mass), the bulk of what we know concerning the IMF—particularly at the low mass end which governs the dynamical behavior of galaxies—is based upon observations of field stars in the immediate solar neighborhood. The local IMF necessarily represents an *average* over a mixed ensemble of stars, some as old as the Galactic disk, which formed in different parts of the Galaxy and in diverse environments.

Fundamental ambiguities plague the determination of the IMF at both its high and low mass ends. At the high end, obvious difficulties stem from the great rarity of massive, very luminous stars. At the low end, the main problem is that the least massive stars are intrinsically very faint and can only be observed in relatively close proximity to the Sun.

The IMF is itself not directly observable, but rather is computed from the luminosity function, $\phi(M_V)$, the mass-luminosity relation, and the bolometric correction. Ignoring the formidable problems associated with determining the mass-luminosity relation, it should be noted that the luminosity function, is the fundamental *observable* quantity for studies of the mass function. It is usually expressed as the frequency distribution of stars per unit volume per unit absolute visual magnitude.

Constructing statistically complete samples of faint (and thus low-mass) main sequence stars in order to estimate the luminosity function has proven to be extremely difficult, even for the immediate solar neighborhood. Studies relying only on stars with measurable trigonometric parallaxes (*cf.* Wicen *et al.* 1983; Henry & McCarthy 1990) have been carried out and necessarily pertain to only the closest ($d < 25$ pc) stars. Other approaches, including those employing kinematic and proper motion constraints (*cf.* Luyten 1963 & 1976; Dahn *et al.* 1986), and optical/infrared photometric surveys (*cf.* Reid & Gilmore 1982; Boeshaar & Tyson 1985; Leggett & Hawkins 1988; Tinney *et al.* 1992) have attempted to extend sample volumes to distances ~ 100 pc. In one extent or another, all these studies are plagued by selection biases and poor statistics, and most possess limiting absolute magnitudes of only 14 - 15 at V.

The luminosity function is poorly understood - and therefore somewhat controversial - for stars with absolute visual magnitudes exceeding 13. For example, the luminosity function computed by Gilmore & Reid (1983) peaks in the range $11 < M_v < 13$, and exhibits a steep decline at higher magnitudes. Interestingly, there is also a suggestion of a rising trend at the extreme low end of the function. The luminosity functions of Hawkins & Bessell (1988) and Leggett & Hawkins (1988) also appear to rise or at least remain flat for masses near the hydrogen-burning limit. 'This is intriguing, since a rising or flat mass function that extends beyond the limit of the minimum mass required to sustain hydrogen-burning would demand the existence of a large number of degenerate brown dwarfs in the Galactic disk. (Given the absence of *any* confirmed brown dwarf candidates, however, it is difficult to avoid the conclusion that even if the IMF continues to rise, for masses $< 0.08 M_{\odot}$, it must soon thereafter steeply decline.)' In any case, recent results suggest that previous surveys which found a decline at the faint end of the luminosity function may simply not have been sensitive to a subsequent 'bump' or rise.

This paper is a study of the faint end of the field star luminosity function, down to limiting magnitudes which correspond to masses near the hydrogen-burning limit, in regions considerably beyond the Solar neighborhood. It implements the approach first suggested by Herbst (see Herbst & Dickman 1983), which relies on deep, multicolor photometry of fields projected against heavily obscured, nearby molecular clouds. Ideally, such clouds act as distance-limiting opaque screens, confining the sample of foreground field stars and minimizing light confusion caused by background field dwarfs and Ia[c]-type giants.

In order to obtain reasonable statistics with this method, one must choose molecular clouds having highly obscured regions of large angular extent. Further, because the search volume probed varies as the cube of the cloud's distance for an opaque region of constant angular area, the requirement that one be able to observe the faintest possible stars with the smallest possible telescope dictates that relatively nearby clouds be selected for study. This was done as follows. Deep multicolor 4-m photography of the Heiles' Cloud 2 region in the Taurus molecular cloud complex, and of 1.1689 in the ρ Ophiuchi cloud (Jarrett, Dickman & Herbst 1989; Dickman & Herbst 1990) revealed the locations and extents of the filaments and cores in these regions with extinctions exceeding 15 magnitudes at V.

To obtain a sample complete to $M_v = 16-18$, requires photometry with limiting visual magnitudes of $-22 - 23$. (Details concerning the data and their acquisition are given in §2). However,

despite their very large extinctions, molecular clouds are not totally opaque at such limiting magnitudes. Color-color criteria must therefore be applied in order to distinguish reddened background stars from inherently red stars located in front of the clouds. This requires that we accurately determine the visual extinctions of the molecular clouds in our sample. We employ star counts to accomplish this (§3). The method of photometric parallax is used to deduce the absolute magnitudes and spectral types of those stars found to lie in front of the clouds. To help further resolve foreground-background ambiguities, we supplement the photometry and color-color results with proper motion measurements of the candidate foreground stars (as outlined in the Appendix), comparing the CCD and photographic data with circa 1950 Palomar Sky Survey fields. These results are discussed in §4. To test the effectiveness of the techniques used to distinguish between foreground dwarfs and heavily reddened background stars, we obtained optical spectra of three candidate stars in Taurus. This work is discussed in §5. We then estimate the field star luminosity function from the Taurus and Ophiuchus fields, and constrain the low mass end of the initial mass function. These results and a discussion of their implications are presented in §6.

2. Observations and Data

The data collected in this program consist of optical photography and CCD images of fields toward the Taurus and p Ophiuchi molecular cloud complexes.

2.1 Photography

Deep prime focus plates in the Kron J, I^c and N bands (Bruzual 1966; Kron 1980) were taken using the 4-m telescopes at CTIO¹ and Kitt Peak¹ during 1983 and 1986, respectively. These plates were used mainly to locate the most obscured portions of each cloud, to estimate their extinctions,

¹The National Optical Astronomy Observatories are operated by the Association of Universities for Research in Astronomy, inc., under contract with the National Science Foundation.

and to form short-term proper motion baselines. The fields observed at CTIO were two $\sim 50''$ diameter areas toward the p Ophiuchi molecular cloud complex, one lying in the southeast filament of the cloud, 1.1689 [$\alpha(1950) = 16^{\text{h}} 30^{\text{m}} 00^{\text{s}}$, $\delta = -24^{\circ} 30' 00''$], and the second in a nearby, nearly extinction-free region [$\alpha(1950) = 16^{\text{h}} 32^{\text{m}} 30^{\text{s}}$, $\delta = -25^{\circ} 00' 00''$]. A single $\sim 50''$ diameter field toward I Icicles'

Cloud 2 in the Taurus molecular cloud [$\alpha(1950) = 4^{\text{h}} 37^{\text{m}} 55^{\text{s}}$, $\delta = -25^{\circ} 46'$] was observed with the KPNO 4-m telescope. All plates were exposed using a Racine prism.

Densitometry of the plates was carried out on the Yale and University of Minnesota PDS machines, respectively. $BVR_K I_K$ photoelectric photometry was also obtained for a number of stars in the cloud and reference regions having apparent magnitudes as faint as 17, using a single-channel photometer on the 60" (1.5-m) CTIO and 50" (1.3-m) KPNO telescopes. These stars were calibrated using a set of Kron standards, the reddest being the M dwarf star Wolf 359 (Gl. 406: $V-R = 1.86$, $R-I = 2.18$; see Bessell 1990). The BVI magnitudes were converted to their J, F, N equivalents using the transformations given by Kron (1980), and the resulting $J, F,$ and N magnitudes for each star were then used to calibrate densitometric diameter-brightness sequences at each color. Because a Racine wedge was used, calibration of the fields was secured to the plate limit in each color. We estimate the accuracy of the magnitude determinations in each band to be ± 0.2 mag.

The end result of this process was a catalog containing the coordinates and J, F, N magnitudes of each star brighter than the plate limits in the cloud and reference fields; $J < 23, F < 22,$ and $N < 19$. These values are not as deep as the plate limits, but represent values at which all detected stars are likely to be real and have apparent magnitudes determined to ± 0.2 mag or better.

2.2 KPNO CCD Observations

CCD images of the Taurus and Ophiuchus fields were made with Tektronix 2048 x 2048 cameras on the #1 0.9-m telescope at Kitt Peak National Observatory. The Taurus observations were carried out in October of 1989, and the Ophiuchus observations were made during May 1990.

Three CCD fields were imaged in Taurus using V, R and I filters. The areas each cover $26' \times 26'$, and are centered at locations (epoch 1950): (1) $\alpha = 4^{\text{h}} 38^{\text{m}} 06^{\text{s}}$, $\delta = 25^{\circ} 36' 10''$, (2) $\alpha = 4^{\text{h}} 36^{\text{m}} 35^{\text{s}}$, $\delta = 25^{\circ} 37' 06''$, and (3) $\alpha = 4^{\text{h}} 38^{\text{m}} 00^{\text{s}}$, $\delta = 25^{\circ} 57' 13''$. The Ophiuchus data set is composed of one $23' \times 26'$ CCD field exposed through V, R and I filters, and centered at $\alpha(1950) = 16^{\text{h}} 29^{\text{m}} 45^{\text{s}}$, $\delta(1950) = -24^{\circ} 23' 00''$. The V and R filters were KPNO standard Harris filters (cf. KPNO 4-m Telescope manual), and the I filter an RG715 (cf. Becker & Newberry 1989).

In order to calibrate the data, a set of Landolt standards (Landolt 1983) was observed. The same standard stars used in the photographic photometry reductions were also imaged using the CCD. The $VR_K I_K$ magnitudes were converted to Cousins equivalents, $VR_C I_C$, using transformations from

Bessell & Weisz (1987). The secondary standards are critical to the calibration, since Landolt standards are generally neither red enough nor faint enough to include heavily obscured stars lying behind the molecular clouds or the least luminous red dwarfs. The Taurus and Ophiuchus secondary standards have (V-J) and (R-I) colors as red as -2.2 magnitudes, but the lowest mass M dwarfs have (R-I) colors that terminate around $-2.2 - 2.4$ mag, redward of the linear calibrations. We are therefore left with little choice but to extrapolate the linear relations $0.1 - 0.2$ magnitudes beyond their measured limit. The potential for systematic errors for the reddest stars therefore cannot be ruled out (this is discussed further below).

Each raw CCD image was subjected to bias and dark current subtraction, flat-fielding and correction for atmospheric extinction. IRAF was used for these corrections, and the extinction coefficients (which were substantial for the Ophiuchus data) were checked against mean site values (see Jarrett 1992); note, however, that no data were taken toward the Oph fields at airmasses > 2 . After these corrections were made, the resulting images were cleaned of cosmic ray hits and cosmetic anomalies and combined into a single, deep exposure for each filter. Individual stellar profiles were then located, isolated, and measured using aperture photometry, and magnitudes assigned at each color.

Errors in the raw stellar magnitudes were estimated from sky and poisson noise, instrument read noise and the number of pixels in the photometry aperture (which depends on the seeing). A less easily quantifiable source of random error derives from the cosmetic quality of the CCD itself. The instruments used in this study were KPNO's first generation of large-format CCDs. Unfortunately these chips have literally thousands of pixels with non-linear responses (*a.k.a.* traps) which misbehave according to the degree of filling of the potential wells (the smaller the filling, the worse the problem). These pixel traps were cleaned from the data when positively identified.

Raw magnitudes were transformed to the Cousins (1976) system using the aforementioned Landolt and secondary standards. As with the photographic photometry, the end result of this reduction process was a catalog containing the coordinates and Cousins V, R, and I magnitudes for each star. Uncertainties in the reduced magnitudes are also included and contain not only poisson contributions, but also a random term arising from errors in the standard calibration; these were estimated from a least-squares analysis of the transformation coefficients. We find the color transformations of (v-r) & (r-i) to $(V-R)_c$ & $(R-I)_c$ to be linear within the scatter of the data to the red limit of $(V-I) = -4.1$. For colors redder than this limit, the transformation may well be non-linear due to systematic effects. A prime source of these are the differences between the CCD filter systems (and

the quantum efficiency of the CCD itself) and the Cousins filter response functions, coupled with the complicated red-band spectra of cool stars (cf. Bessell 1986; Taylor 1986). The response functions of the Harris R filter used with CCD detectors at KPNO and the corresponding Cousins filter are slightly different at long wavelengths². These differences are magnified upon convolution with a

² The extended tail of the Cousins R filter response, ranging to $\sim 9000 \text{ \AA}$, compared to the more rectangular Harris R filter response which cuts off at $\sim 8500 \text{ \AA}$, "conspires to systematically brighten a cool red star measured using a Cousins R filter relative to what is measured using the Harris filter. The filter response function of the RG715 filter has an I-band response characterized by a sharp cutoff at the blue end ($\sim 7000 - 7200 \text{ \AA}$), similar to the Cousins I filter, peaks at $\sim 7500 \text{ \AA}$, and ramps downward to $\sim 10000 \text{ \AA}$. Since the Cousins I filter is mostly rectangular, the RG715 I band filter will be more sensitive to the flux of a cool star.

late-type dwarf spectrum, where deep molecular absorption features appear between the R and I filters and, particularly, within the I-band filter itself.

To summarize, for both the Taurus and Oph data sets, we measure V-band limiting magnitudes of 21.2 ± 0.1 and 22.2 ± 0.2 . At the bright end, calibration to the Cousins systems results in a photometric uncertainty limit of 0.03 - 0.04 mag. The R and I data have limiting magnitudes of 21.0 ± 0.01 and 20.5 ± 0.1 , respectively; thus, since most of the stars in the fields are heavily reddened, the (V-R) and (R-I) colors have uncertainties of up to 10% for $V \leq 21.5$ to 22.0. In this study, we limit our analysis to stars with (R-I) color uncertainties $\leq 10\%$ - in this case, V magnitudes may have uncertainties as high as 17%.

3. Star Counts and Visual Extinctions

In this work it is of central importance to determine the distribution of visual extinction over the molecular clouds which delimit the fields selected for study. Only if the visual extinction is known, can a background star's colors be dereddened, thereby allowing constraints to be placed on its spectral type, luminosity class; a star closer than the molecular cloud will have little or no reddening, so that attempting to deredden its colors will place it in an unphysical region of the color-color plane.

Extinctions due to the molecular clouds were estimated using the method of star counts (SCC Bok 1956; Dickman 1978). The extinction at each color was initially determined over areas $1' \times 2'$ on a side; mean extinctions for larger star-free regions were computed according to the prescription given by Dickman.

All stars were treated as background objects. In principle, this means that the extinctions determined at each location in the clouds are only lower limits. However, for any reasonable values of the luminosity function, it is easy to show that because the Taurus and Ophiuchus clouds are so close, this simplifying assumption has virtually no practical impact on the results of interest here. The details of the extinction determinations varied somewhat between the two cloud fields, and are discussed separately below.

3.1 Taurus

Even the most lightly obscured areas within the photographic and CCD fields for Taurus have significant extinction. Accordingly, we chose as a fiducial reference field the $5'$ square area centered on location $\alpha(1950) = 4^{\text{h}} 39^{\text{m}} 45^{\text{s}}$, $\delta = 25^{\circ} 45'$, and initially expressed all photographic extinctions relative to this region. The residual extinction within this boundary was separately determined to be $A_v \approx 1.7$ mag, as described by Jarrett (1992), and this value subsequently added to all extinctions determined relative to the fiducial reference. The CCD fields did not include the fiducial region. We therefore chose as CCD reference fields two $4' \times 6'$ boxes centered at $\alpha(1950) = 4^{\text{h}} 39^{\text{m}} 05^{\text{s}}$, $\delta(1950) = 25^{\circ} 45'$, and $\alpha(1950) = 4^{\text{h}} 38^{\text{m}} 55^{\text{s}}$, $\delta = 26^{\circ} 05'$. As a first approximation, we expected the residual extinction within these areas to be the same as that in the photographic reference field. A more exact treatment, using a starcount model of the Galaxy (Jarrett 1992) gave a slightly higher residual extinction of 2.0 mag.

Star counts at I provide the greatest penetration of the cloud. We divided the I band CCD field into a grid of resau cells in $1.4' \times 1.4'$ size. In each square, the number of stars with apparent magnitudes brighter than 20.8 was counted and scaled to a corresponding area of 1 deg^2 . Those resau cells with no stars were assigned a count of 1, and contiguous areas of zero star counts were assigned, as a group, one count. The effective extinction toward each square at I is then found from the reference fields described above. Visual extinctions were computed, using the reddening law of Savage & Mathis (1979): $A_v \approx 1.69 A_I$. The resultant visual extinction map was then smoothed using a sharply-peaked 3×3 gaussian filter. This reduced the statistical errors associated with the most

obscured portions of the cloud and effectively smoothed the abrupt transition between regions with moderate extinction and those with extinction set by the lower limit. (This sharp gradient is non-physical, and is due to the way that small sample statistics are treated and to the discreteness of the star counts.) A grey-scale image of the visual extinction map determined for the Heiles' Cloud 2 CCD field is shown in Figure 1, overlaying the map arc contours of $A_v = 5$ and $1()$. The extinction values range from 2 to a lower limit 23 magnitudes.

3.2 Ophiuchus

The photographic data includes a 50' diameter reference field, exposed at the Kron J, F and N bands, and centered at $\alpha(1950) = 16^h 32^m 30^s$, $\delta = -25^\circ 00' 00''$. Dickman & Herbst (1990) used this data to correct for the residual extinction at the edge of the cloud field proper. Profiles of the cumulative stellar surface density curves, corrected for residual extinction, at all three colors can be seen in Dickman & Herbst (1990). In their study, the N-band star counts provided the deepest measure of the extinction, largely due to the longer wavelength ($\lambda_0 = 7941 \text{ \AA}$); the N-band plate limit was conservatively adopted to be 19.5 mag. We used the N-band star counts of the Ophiuchus reference field to calibrate the CCD images exposed at Cousins I band.

The I-band CCD field covers a 23' x 26' area centered at $\alpha(1950) = 16^h 29^m 45^s$, $\delta = -24^\circ 24' 10''$. The field was divided into a 21 x 19 resau grid with cells of size 1.25' x 1.25'. In each cell, the number of stars with apparent magnitude brighter than 20.4 was counted and scaled to a corresponding area of 1 deg². Resau cells with no stars were assigned a count of 1, and contiguous areas of zero star counts were assigned, collectively, one count. The effective extinction toward each square was then easily determined.

The same factor as in the case of Taurus was adopted to convert the I-band obscurations to visual extinctions. The resultant visual extinction map was then smoothed using a gaussian filter. A grey-scale representation is shown in Figure 2, with contours of $A_v = 5$ and $1()$ shown. The visual extinction is as low as 3-5 mag at the outer perimeter of the field, and extends to more than 21 mag within the interior. The darkest regions have contiguous cells with no stars brighter than the plate limit.

4. Color - Color Analysis

A key advantage of using photometric methods to search for low mass stars is the technique's freedom from kinematic and population biases (*cf.* Hanson 1983). Further, by using multi-color photographic or CCD photometry, large areas with deep limiting magnitudes can be surveyed - typically, the resultant search volumes are at least an order of magnitude greater than that of parallax surveys. However, although photometric colors can be used to discriminate between stars of different spectral type, there may be some ambiguity between luminosity classes. This effect can be minimized by studying fields in the direction of nearby molecular clouds: Ideally, stars behind the cloud will be either completely blocked from view or so heavily reddened that [their colors will reveal this. In principle, this permits us to isolate a complete sample of low mass stars - provided the photometry is sufficiently deep - within the volume defined by the survey area and the distance to the cloud. In practice, we shall see that with the deep photometric data used here, ambiguities remain in distinguishing extreme M dwarf foreground stars from earlier, reddened background objects. An additional potential complication is the possible presence of late (or moderately late) type stars, formed *within the* molecular cloud itself - in this case the value of the reddening suffered by the star is bounded, but essentially indeterminate.

We may demonstrate the opaque screen method using the Taurus extinction map (Figure 1) and a Galactic stellar distribution model. The stellar distribution model predicts the surface density of stars for a given direction in the Galaxy, providing the expected total number of stars per spectral type heated within a given solid angle, as a function of limiting magnitude. We have assumed a local stellar number density based on previous determinations of the luminosity function (e.g., Wielen *et al.* 1983). Information contained within a single simulation includes population type (type I: disk, and type II: spheroid or halo, with spatial functional forms prescribed by Bahcall & Soneira 1980), spectral type, luminosity class (main sequence dwarf and evolved giants), apparent magnitudes, colors and locations. We have applied a random noise function to the model photometry that matches the empirical values determined for the Taurus data set (see §2). Finally, we have corrected stellar colors for the non-linear effects of interstellar extinction using a synthetic technique that convolves stellar flux distributions with the non-rectangular filters used in this study. Further details of the galactic distribution model and the synthetic photometry method are given in Jarrett (1992).

in this demonstration we would like to model the surface density of stars that are situated along the line of sight toward the Taurus molecular cloud³. First consider the case in which the cloud³ in the case of ρ Oph, the stellar number density is greater than Taurus (since the ρ Oph is only ~ 100 from the Galactic center); however, the results are similar in both cases.

dots not interfere with the light from distant stars in the Galaxy. The predicted number of stars brighter than the CCD V-band limit, -22.2 , located along this line of sight ($Q = 173^\circ$, $b = 13.6^\circ$) is ~ 17000 stars deg^{-2} . A histogram showing the distribution of absolute magnitude, M_v , for these stars is displayed in Figure 3a. It is interesting to note that while M dwarfs are the most common stars in the Milky Way, the bulk of the field stars shown in the histogram are G and K dwarfs. This effect is a reflection of a luminosity and volume bias. An important feature to note from the histogram is that late M dwarfs ($M_v > 12$) are predicted to be present in about the same numbers as evolved giant stars. Given that M giants have roughly the same colors as their dwarf counterparts, it is clear that in the absence of a molecular cloud, it would be difficult to separate the two classes of stars based on photometric constraints alone. Now consider the case in which the molecular cloud acts as an opaque screen to stars located behind the cloud. We adopt a distance of 140 pc to the Taurus cloud (Blais 1978a). The visual extinction of the Heiles' Cloud 2 region varies from 2 to at least 21 magnitudes, with an average of $\sim 5-17$ mag. The total number of stars brighter than the CCD limiting magnitude is now ~ 1600 deg^{-2} . In Figure 3b we see that the cloud also directly affects the shape of the observed stellar distribution. The histogram of reddened field stars is now dominated by G dwarfs. In addition, luminous giant stars are elevated in number density with respect to the dwarfs; i.e., the cloud acts as a bias toward distant, luminous stars, while isolating the unreddened population of stars located in front of the cloud.

As discussed in §2, we are concerned with possible systematic effects in the color transformations, particularly at the red end of the VRI color plane. Hence, it is constructive at this point to compare the model (V-R) & (R-I) colors with the actual Taurus data. The comparison was made by superimposing the Taurus (V-R) & (R-I) data on the monte-carlo data that was generated via multiple trials. We find no evidence for a systematic error in the Taurus color data to within 5% or so. Models specific to the Ophiuchus data are also consistent with this result.

4.1 Taurus Sample

While the limiting magnitudes of both the CCD and photographic data sets for Taurus are comparable, the CCD photometry is superior, with a limiting accuracy of $\pm 1\%$, compared to the 20-25% for the photographic photometry. The remaining analysis therefore considers only the three $18' \times 26'$ CCD fields. Within this area about 2600 stars are detected at V, R or I, and 1650 were detected at all three bands with at least a 10:1 S/N ratio for the (R-I) index. Another 20 stars or so were bright enough to saturate the CCD and were discarded from further consideration. The resultant range in apparent magnitude was $13 < V < 22.2$, $13 < R < 21.5$, and $13 < I < 20$. Since the opaque screen method functions best when the cloud extinction is high, we restrict our attention to areas of the cloud where the visual extinction is at least 3 mag. (We chose this value so that the minimum extinction in the Taurus sample is identical to that for the Oph field.) About 34% of the sample remained for study after this criterion was imposed. In Figure 4 we plot the colors of all stars detected at V, R, and I. Nearly all lie above the main-sequence and giant tracks shown in the figure⁴, *i.e.*, most stars

⁴ The data were obtained from Bessell (1991) and Johnson et. al. (1966). Conversion from the Johnson photometry system to that of Cousins (1980) was performed using calibrations of Fernie (1983). The colors represent typical values for each spectral class up to and are to discern the relative location of the unreddened sequence. For the most extreme red dwarfs, $(R-I) > 2.3$, the mean colors are very uncertain; the little evidence that is known about the stars suggests that the colors are actually bluer than expected.

are scattered along the reddening curves expected for background field stars. There are also a few stars with colors well *below* the main-sequence. We discuss these in more detail at the end of this section.

Based upon a star count model (see §4) the dominant fraction of stars in Figure 4 are expected to be background G and K dwarfs; stars fainter than $V \sim 18$ most likely to be heavily reddened disk dwarfs located behind the cloud at distances < 1 kpc. Many of the stars in the figure are unambiguously reddened and can therefore be discarded from further consideration as foreground candidates. Still, this leaves a large fraction of stars with color-color locations within 0.1 to 0.2 magnitudes of the main-sequence track. We need to apply yet another criterion to this sample in order to cull the foreground stars from the reddened background populations.

Photometric parallax provides a method to isolate objects whose colors and apparent magnitudes are consistent with their being closer than the molecular cloud. Since a foreground star will suffer negligible extinction at 1, its absolute magnitude can be determined by assigning the *most likely* spectral type based on the observed (V-R) and (R-I) colors. Since most data points in Figure 4 do not lie on the average main sequence track, the least biased approach is to simply determine the nearest point on the main sequence track, hereafter represented by the subscript 0, as in $(V-R)_0$ and $(R-I)_0$. We can then assign a spectral type and absolute magnitude using $(V,R,I)_0$ and the mean M_1 vs. (R-I) relation, given in Bessell (1991). If the distance implied by the apparent and absolute magnitude is greater than that of the cloud (140 pc), the colors and apparent magnitudes are not consistent with a foreground star interpretation and the star is excluded from further analysis. Note that the absolute magnitude-color relation has an intrinsic spread, which, effectively increases the uncertainty in the deduced distance as does the uncertainty in the observed magnitude of the star. In addition, Bessell points out that the M_1 - (R-I) relation is uncertain for the most extreme M dwarfs, with $(R-I) > 2.3$.

To implement the method described we note the following. First, the faint end of the unreddened V,R,I color plane is bounded by the color limits of the lowest mass stars, $(R-I)_0 < 2.4$, and $(V-I)_0 < 2.2$ (Bessell 1991). Allowing for 10% photometric uncertainty, we extend this boundary another 0.1 magnitudes. Stars with more extreme colors are rejected from further consideration. Second, we must set a limit to the extent that the stellar colors can deviate from the mean main-sequence track. For clarity, let ζ be the minimum magnitude difference between the stellar colors (V-R) & (R-I), and the corresponding main-sequence color, $(V-R)_0$ & $(R-I)_0$ of an observed main sequence star. The maximum allowed difference, ζ_{max} , between (V,R,I) and $(V,R,I)_0$ defines the limit at which we cull the data with the photometric parallax criterion: if $\zeta \leq \zeta_{max}$, we then apply the photometric parallax method to data point, otherwise we discard it from further consideration. In principle, ζ_{max} should be small in order to minimize the confusion caused by distant, reddened stars that -- by chance -- have colors and brightnesses consistent with spurious identifications as nearby low mass stars. On the other hand, ζ_{max} must also be large enough so that all true foreground stars are included in the photometric parallax criterion test. With 10% photometry, a foreground star will have colors that at least two-thirds of the time scatter within 0.1 magnitudes of the main-sequence track. We therefore provisionally adopt a ζ_{max} of 0.1.

A more rigorous justification for selecting this value of ζ_{max} is to employ a stellar distribution model that includes model photometric limits and uncertainties similar to the observed data. We will

consider both cases described in §4, apply the photometric parallax test to the simulated color-color data using ζ_{max} as the independent variable, and compute two critical ratios. The first gives the fraction of foreground stars (i.e., $D < d_{\text{cloud}}$, where D is the true distance) that lie within the ζ_{max} envelope and have photometric parallaxes $d < d_{\text{cloud}}$. This ratio represents the detection frequency of foreground stars with our method. The second ratio gives the fraction of *background* stars - relative to the total foreground candidate sample -- that lie within the ζ_{max} envelope and have $d < d_{\text{cloud}}$. This ratio represents the frequency of false detections. The results of these calculations are shown in Figure 5. Without cloud obscuration (Figure 5a) the percentage of false detections is an unacceptably high ~80%, regardless of ζ_{max} . The bulk of the sample contamination comes from K dwarfs located some 2(X) to 400 pc from the Sun that have colors mimicking those of low mass red dwarfs. Figure 5b demonstrates the effectiveness of the opaque screen method. Nearly all of the foreground stars are detected within a 0.1 magnitude ζ_{max} envelope, while most of the background K and M dwarfs are screened away by the Taurus cloud. The contamination of the foreground sample by background stars is -15% for $\zeta_{\text{max}} = 0.02$, and slowly rises to -30% at $\zeta_{\text{max}} = 0.10$. The contaminants are mostly F and G stars ($M_V = 3 - 6$) located within 1 kpc of the Sun. The (reddened) colors of these stars mimic foreground M0 dwarfs, whose location on the VRI main sequence track corresponds to the point at which the (R-I) color begins to dominate for the cooler stars (this is significant because the slope in the main-sequence track at this point departs from the reddening vector). In addition, contamination at the 10 - 15% level is due to background M1 and M2 dwarfs ($D < 300$ pc) whose simulated colors mimic those of very late-type M dwarfs, in the bins corresponding to $M_V = 15 - 17$.

We conclude from Figure 5b that the opaque screen method is effective in separating low mass foreground stars from more distant stars located behind the molecular cloud. One must use caution however, when counting the inferred foreground stars belonging to the faintest absolute magnitude bins. Given the photometric accuracy of this study, these bins may have a false detection frequency of up to -15% of the total.

Adopting 0.1 as the maximum limit to ζ , we have culled the Taurus data plotted in Figure 4. Results of this effort are shown in Figure 6, in which we have highlighted stars with foreground solutions (large filled circles): These stars have colors, apparent magnitudes, and inferred absolute magnitudes consistent with their being low-mass luminosity class V objects located in front of the Taurus molecular cloud. Their photometric properties are given in Table 1. Included in the table are the equatorial proper motions, and their estimated errors (see Appendix for description of the technique

we used to measure proper motions). It can be seen from the table that nearly all of the foreground candidates have relatively large proper motions, exceeding $3'' \text{ cent}^{-1}$, consistent with their being located nearby (partially due to reflex motion of the Sun); in comparison, field stars located beyond the molecular cloud should exhibit proper motions less than this value.

Also shown in Figure 6 (as filled triangles) are either resolved doubles or triples, or objects with elongated profiles. The latter objects may be unresolved multiple systems or young stars associated with the molecular cloud. (For example, the $H\alpha$ object, Haro 6-33, $V-R = 1.37$, $R-I = 1.54$, exhibits a well defined 'tail' or optical jet structure.) The resolved doubles are objects with two clearly separate stellar profiles, but which are spatially too close (within $6''$) to allow reliable measurement of their separate fluxes. These objects may in fact be physically associated systems, or alternatively, simply chance superpositions. The latter appears likely, since most of the objects are bright-faint pairs, with the faint companion very red relative to the bright companion (in many cases the faint companion is not detected at V); also, the color-color distribution of these objects lies primarily along the expected reddening track. It should also be noted that one of the foreground candidates, #1433, is located $9''$ from a faint reddish star. The faint star's fluxes at R and I are, unfortunately, inseparable from those of 1433, so it is not possible to conclude whether this star is physically associated with 1433 or is simply a distant star shining through the cloud (subject to $A_V = 3$).

Eight stars in Figures 4 and 6 have unusual colors. In Table 2 we list the photometric properties of these stars. Stars #90, 626, 1136, and 1543 have $(V-R)$ colors well below the main-sequence track. These stars are quite faint, with rather large color uncertainties, $> 10\%$, which suggests that they may be scattered $2 - 3\sigma$ from the main sequence or expected reddening track. For #90 we measure a very high proper motion, $40'' \text{ cent}^{-1}$, which if correct, strongly implies that this star belongs to the spheroidal or halo population; however, this measurement should be regarded with caution since this star is very faint (near the limit of the POSS survey) and its large proper motion may instead reflect a false match between our CCD data set and the POSS survey (see Appendix). The most interesting stars in Table 2 are the extreme red objects, #32, 847, 893, and 1004, which have colors redward of the late M dwarf sequence. These stars may be associated with the cloud or may be very low mass stars with colors 1 or 2σ away from the nominal (but uncertain) values for M7 - M8 dwarfs. Two of the stars, 847 and 893, are in close proximity to the T-Tauri star GN Tau (Haro 6-31) and one of the dense, "ammonia" cores of the cloud (cf. Myers *et al.* 1983; Cernicharo & Guelin

1987). As Beichman *et al.* (1986) point out, nearly half of all dense cores in molecular clouds have associated T-Tauri stars and/or embedded protostars (as evident in the far-infrared IRAS sources). Further, none of the four exhibits appreciable proper motion. '1'bus, although they do not qualify as obvious foreground candidates, [they are probably worth additional study via near-infrared imaging or spectroscopy.

4.2 Ophiuchus Sample

As in the case of the Taurus color-color analysis, we consider only the CCD data here. The data consist of a single $23' \times 26'$ CCD field. A total of ~ 700 stars was detected at V, R, or I. Of this sample, ~ 200 were detected at all three bands with at least a 10:1 S/N ratio in (f<-]). Due to non-linear CCD saturation effects, ~ 10 stars brighter than $V = 12$ were discarded from the sample. The resultant range in apparent magnitude is $13 < (V, R) < 22.1$, and $13 < I < 20.5$.

In Figure 7, we present the CCD photometry of these stars in the VRI color-color plane. As in the Case of Taurus (Figure 4), most Of the stars appear to cluster about a reddening **Curve**. As before, in order to better understand these properties a monte-carlo simulation which convolves the extinction distribution in the field with our Galactic model (Jarrett 1992) was carried out for all three color bands. As expected, reddened background dwarfs were found to dominate the observed star counts; about 10 times as many stars are detected at I-band than at V. Stars with $V > 18$ are most likely G - K dwarfs, and stars near the limits of the photometry are almost certainly dwarfs located behind the cloud, within 1 kpc of the Sun,

The procedure to refine the foreground candidate sample further is the same as that described above for Taurus. For each star, the nearest point from colors (V-R) & (R-I) on the main sequence was ascertained, and appropriate mean main-sequence colors $(V-R)_0$ & $(R-I)_0$ assigned. If the magnitude difference, ζ , between the color pairs is less (then 0.10), then applied the photometric parallax criterion. Derived distances less than that of the Ophiuchus molecular cloud, ~ 160 pc (Elias 1978 b; de Geus 1988) imply that the star can be consistently identified as a foreground object.

Results are shown in Figure 8. Foreground candidates are denoted by filled circles, and visual doubles and/or candidate stars associated with the molecular cloud are represented by filled triangles. The photometric and inferred physical properties of these stars are given in Table 3. As in the case of the Taurus foreground candidates, nearly all of the Oph foreground candidates exhibit proper motions exceeding $3'' \text{ cent}^{-1}$. Four objects that are too red **to** include in this list yet **are** worthy of mention:

#25, 34, 42, and 59. The location of these objects in the VRI plane, $2.4 < (V-R), (R-I) < 2.6$, might suggest that they are extreme low mass stars or even degenerate objects. On the other hand, the simplest answer is that they are heavily reddened objects. The latter is more likely given that these stars are faint ($V = 21$ to 22) and two of them, #42 and 59, have extremely red infrared colors (we discuss these measurements below). Stars 25 and 59 have relatively large proper motions, $\sim 4'' \text{ cent}^{-1}$, but they are only 2σ measurements. The other two stars have little or no proper motion.

Another object of interest is #13, which has relatively blue colors, $(V-R) = 0.20 \pm 0.04$, $(R-I) = 0.54 \pm 0.03$. However, even though this star is 'blue', $(R-I)$ is 0.2 to 0.3 mag redward of a color expected of white dwarfs (Bessell 1990). Given its visual brightness, 17.28 ± 0.05 , blue colors and relatively small uncertainties in the VRI colors, it seems unlikely that this star is located behind the Ophiuchus cloud. Unless the measured values are in gross error, it would seem that the object is an unresolved white dwarf - red dwarf system. Indeed, at R and particularly I , the stellar profile of this object is clearly oblate. Choosing the following parameters

white dwarf, $M_v = 12.30$, $(V-R) = 0.10$, $(R-I) = 0.10$

red dwarf, $M_v = 16.65$, $(V-R) = 1.91$, $(R-I) = 2.22$

implies that at 100 pc, the system will have a combined visual magnitude of -17.28 , and $(V-R) = 0.18$, $(R-I) = 0.56$. This solution is, of course, not unique, but it is likely that the unresolved red companion is as late a type as $dM6$, with the pair located ~ 100 pc from the Sun. The binary object has a measurable proper motion of $11 \pm 2'' \text{ cent}^{-1}$. If the object is located 100 pc from the sun, then the transverse velocity would be $\sim 50 \text{ km s}^{-1}$, which is plausible given the high mean dispersion velocity of white dwarfs.

4.3 Other Surveys of the ρ Ophiuchi Region — Constraints on Foreground Stars

A number of studies have been carried out in the x-ray (*cf.* Feigelson 1987; Montmerle *et al.* 1983), optical (Ichikawa & Nishida 1989), infrared (e.g. Wilking & Lada 1984), and radio (Andre *et al.* 1987; Stine *et al.* 1988) to detect and identify young stellar objects in the ρ Oph complex. Wilking & Greene recently surveyed the northern portion of 1.1689 at J, I and K (private communication). About 40% of their survey overlaps our CCD field, with 18 stars common to both studies (Jarrett

1992). Of these stars, two are identified with optical foreground candidates from this study, #92 and 587, and an additional two correspond to the extreme red stars, #42 and 59, discussed previously. The foreground candidates, 92 and 587, have (V-K) colors of 5.0 and 2.6, respectively, consistent with the spectral type inferred for these objects using the method outlined in this paper. In contrast, the other two stars (#59 and #42) have very red infrared colors ($J-K > 3$) suggestive of heavy intervening extinction. The #42 is in fact, a double visual and infrared source; and is associated with a 25 μ m IRAS point source, IRAS 16293-2424. This object also lies $\sim 2'$ south of the IRAS source 16293-2422 – identified with an energetic high-velocity bipolar molecular outflow (Walker *et al.* 1986; Mundy *et al.* 1986). The close proximity of #42a,b to this outflow source, as well as its sharply rising flux density toward the far-infrared (see Jarrett 1992) strongly implies that this object is associated with the group of newly forming stars neighboring the outflow source.

In addition to the two IRAS point sources noted above, [here are four other very faint IRAS sources in the L1689 field (see Beichman, Boulanger & Moshir 1991). None of these additional sources are associated with optical detections from this study or infrared detections from Wilking & Greene.

4.4 Stars with only R and I Detections in Taurus and Ophiuchus

The vast majority of stars detected in our Taurus and Ophiuchus CCD observations do not have V-band counterparts. Since most are background objects, this is expected -- the presence of the molecular cloud biases the survey toward detections of heavily reddened, intrinsically red stars. However, most of the essentially conical volume populated by foreground stars is close to the molecular cloud, so that extremely late M dwarfs may be missed at V if they are close to the cloud. Thus, a small percentage of the stars detected only at R and I may be foreground objects. Unfortunately, spectral classification is nearly impossible when only one color is available. Nevertheless, we may cull the R, I sample of stars whose properties are inconsistent with those of unreddened, late M dwarfs by using not only the (R-I) color, but also the I magnitude, cloud distance modulus and visual extinction.

The procedure follows a number of steps. Two observational properties constrain the R, I detections: (1) the limiting visual magnitude of the data is ~ 22.2 , and (2) the distance modulus to both clouds is ~ 6 . As noted above, any foreground stars not detected at V are most likely located near the cloud since a conical search volume grows quadratically with distance. At the cloud distance, our

survey is thus strictly complete only to an absolute visual magnitude of -16 – -17 , corresponding to an M5.5 or M6 V star. A star of this spectral type will have a mean (R-I) color -2.2 . A star with an (R-I) color greater than this value will not be detected at V (unless it is closer than 150 pc), but *will* be detected at R and I. Moreover, stars with (R-I) color greater than -2.5 are probably not red dwarfs, because this color index ceases to increase with spectral type for the latest M dwarfs (Bessell 1991). All stars satisfying the constraints specified above can be further culled by assigning an absolute magnitude, M_I , via the color index and comparing the distance modulus of the cloud with the derived stellar distance. Stars found to be closer than the cloud modulus have properties at least self-consistent with their being late-type M dwarfs. Again, we caution the reader that the inferred M_I is very uncertain for extreme red dwarfs. The value we derive from (R-I) is only a rough estimate of the true value (which may range from 12.5 to 14.5).

Unfortunately, most of the (R-I) stars have properties not only consistent with their being foreground stars, but also with their being reddened background G and K dwarfs. This is the major limitation of one-color analysis - there are usually two solutions. However, there appear to be no acceptable background stellar solutions for a few of the (R-I) stars. Tables 4 and 5 list the photometry and color solutions for Ophiuchus and Taurus stars, respectively, satisfying the constraint $2.2 < R-I < 2.5$, consistent with late-type M dwarfs in the range M6 - M8 V.

5. Spectra of Three Taurus Candidates — A Check on Methods

During December 22 and 23 of 1990, three of the Taurus foreground stars⁵, #604, 823 and

⁵Two of the stars, #604 and 823, were selected from the foreground candidate sample (Table 1) based on their colors and high proper motions; object #994, whose colors would indicate foreground candidacy if $\zeta_{\max} = 0.15$, was selected primarily due to its very high proper motion.

994, were observed at the authors' request by Terry Lerner of Cornell University using a grating spectrograph and the 4-Shooter CCD camera on the 5-m Hale Telescope of Palomar Observatory. The spectrograph covers a wavelength range from 6000 Å to 9000 Å and uses a 300" line/mm grating, which yields a spectroscopic resolution of ~ 15 Å. A slit width of 2" x 1.5" was employed. The data reductions were carried by one of us (T.H.J.); the images of the spectra were flat-fielded, bias-subtracted, sky-subtracted and converted to one-dimensional spectra using the routines in the IRAF

software analysis package. The spectra were wavelength calibrated using a He-Ne-Ar reference spectrum and were flux calibrated using IIDS standard stars and various IRAF routines. Strong absorption features attributed to terrestrial O_2 at 6800 \AA and 7600 \AA , and H_2O at 7200 \AA were not removed from the spectra.

Because of contamination from the telluric absorption features, it is difficult to measure TiO and V() band equivalent widths precisely. Accordingly, we favor spectral classification of these stars *via* qualitative comparisons between temperature and gravity-sensitive features with those of the Bessell (1991) and Kirkpatrick, Henry & McCarthy (1991) M dwarf spectral sequence, and with those of the spectrum of the late M dwarf, Wolf 359 (Gl 406), Figure 9 (data provided courtesy J. Stauffer). The spectra of stars #604, 823 and 994 are shown in Figures 10 - 12, respectively.

S.1 Spectrum of Candidate #604

The most striking properties of the spectrum of #604 are the rising flux continuum toward red wavelengths, and the numerous absorption features blanketing the continuum. Major TiO features, including the TiO bands at 7200 \AA , 8300 \AA and 8500 \AA , are present, strongly suggesting that this star is very cool; the strengths of these bands are comparable to those in stars with a spectral type later than M4. Furthermore, there appears to be a hint of molecular VO at 7500 \AA and particularly, at 7900 \AA , but longward of 8500 \AA it is impossible to distinguish between absorption features because of the poor signal to noise. Overall, the spectrum suggests a temperature class corresponding to that of an MS star, but probably no later than M5.

The spectrum undoubtedly corresponds to that of a dwarf because of the many tell-tale gravity-sensitive features prominent in the spectrum, including CaOH I at 6250 \AA , possibly Ca I at 6400 \AA , K I at 7700 \AA , and the prominent Na I feature at 8200 \AA . The strength of the sodium feature itself suggests that this star is at least as late as M4 and is probably an MS dwarf. Finally, $H\alpha$ emission is prominent in the spectrum of #604, hinting at significant chromospheric activity, and thus, is also consistent with this star being a late-type M dwarf.

Based on the spectral evidence outlined above, we favor the classification of candidate star #604 as a MS V or M6 V, where the spectral type MS V is probably the better estimate. An MS dwarf has the following properties:

$$M_V = 14.7 \text{ and } M_I = 11.3,$$

$$V-R_c = 1.5 \text{ and } R_c-I_c = 1.9 .$$

These **values** are consistent (to within **-1 (0%)**) with the observed broad band colors and deduced luminosities for foreground candidate #604 (see Table 1).

5.2 Spectrum of Candidate #823

The spectrum of foreground candidate #823 is similar to that of #604, in that it is clearly a cool star. Fortunately, the S/N is considerably better for this star, and thus, it is easier to identify molecular and atomic features. Comparing its spectrum with that of #604, we see that the TiO features at 8500 Å and W(K) Å are equally prominent (and better defined), and, more significantly, there is a hint of the VO bands at 7500 Å and 7900 Å for #823. Indeed, the molecular features in the spectrum of star #823 **are similar to those seen in** the spectrum of Gl. 406 (Figure 11), an M6 dwarf. Several gravity-sensitive features **are present in** the spectrum of #823, including CaOH at 6250 Å, Ca I at 6900 Å (though there is contamination from the O₂ telluric band), K I at 7700 Å, Ca II at 8500 Å (with contamination from the nearby TiO band), and finally, a prominent H α feature at 8200 Å. As in the case of #604, **there is also a significant H α emission line.**

Based on the gravity features and the strengths of the TiO and VO bands, we favor the classification of this star as a dwarf of spectral type between M5.5 and M6. An M6 dwarf has the following mean properties (Bessell 1991):

$$M_v = 16.6 \text{ and } M_I = 12.5,$$

$$V - R_c = 1.9 \text{ and } R_c - I_c = 2.2.$$

These values are consistent (to within ~10%) with the observed broad band colors and deduced luminosities of foreground candidate #823, listed in Table 1.

5.3 Spectrum of Candidate #994

Although star #994 [$V = 19.69 \pm 0.09$, $(V-R) = 1.70 \pm 0.07$, $(R-I) = 1.92 \pm 0.04$] is not one of the foreground candidates (it has a ζ value of 0.14), it does appear to have a large proper motion and as such we chose this star for study. The spectrum of 994 is markedly different from those of the previous two foreground candidates. In particular, it is noticeably lacking in molecular features. The features at 6900 Å, 7300 Å and 7600 Å are probably due to terrestrial oxygen and water absorption; however, there is a hint of the TiO bands at 7200 Å and 85(K) Å. Furthermore, it is difficult to identify any gravity-sensitive features. There may, however, be some H α emission at 6563 Å, although this is difficult to discern. Based simply on the relatively weak molecular bands, this star

probably is not very late in spectral type. On the other hand, the continuum flux is clearly rising beyond 9000 \AA , indicative of interstellar reddening. The projected location of the star #994 on the Taurus molecular cloud **corresponds to a visual** extinction of about 5 mag and $A_V \sim 3$ mag. If this object lies behind the cloud, then flux at 9000 \AA is differentially *elevated* with respect to the flux at 6000 \AA by a factor of ~ 6 . If we account for this [then the spectral continuum of #994 is more or less flat, which is consistent with its being a K5 or M0 star.

Let us consider this hypothesis in conjunction with the observed photometric properties. If the star is a K5 dwarf, then its intrinsic visual magnitude must be -7.6 . The apparent visual magnitude (extinction-corrected with $A_V \sim 5$) is -14.7 , and thus, the deduced **distance** from the Sun is about 260 pc, which is a reasonable location for a Galactic disk dwarf. Even if the star is an M0 dwarf, its intrinsic magnitude is ~ -8.8 , and the resultant distance is ~ 150 pc, still beyond the cloud (though the close proximity of the star and cloud raises the possibility of some kind of association).

If the star is a K5 III giant, then its absolute magnitude is ~ -0.3 , and the deduced distance is ~ 7.6 kpc, which would imply a Z height > 2 kpc. Even if we take into account general interstellar absorption of -1 mag per kpc which is appropriate for the Galactic plane, the deduced distance is beyond 4 kpc. Therefore, we consider the field dwarf interpretation as the more likely scenario.

Star #994 has a significant proper motion of $(\mu_\alpha \cos \delta, \mu_\delta) = (2.5 \text{ \& } 6.7) \text{ cent}^{-1}$, giving a total proper motion of $7.1 \pm 1.3 \text{ cent}^{-1}$. If our interpretation that this star is a field dwarf located at a distance between 150 and 260 pc from the Sun is correct, then the deduced tangential velocity must be in the range from 50 to 90 km s^{-1} . A (dispersion velocity of this magnitude is possible for what could be expected for old disk K and M dwarfs - though on the **high** end, perhaps $\sim 2\sigma$ from the typical value. Another possibility is that this star is a K5 subdwarf belonging to an intermediate or spheroidal population. This is, however, less likely given that there is no evidence for strong Ca I bands (indicative of extreme subdwarfs, see Ake & Greenstein 1980) in the spectrum of 994. In any case, this star is clearly not a low mass M dwarf. This is significant in that if we had extended the ζ envelope (see Figure 6) to 0.15 mag, then this object would have been classified (falsely) as a nearby dM5 star. Apparently the 'contamination' rate implied in Figure 5 is to be taken seriously.

To summarize, a spectral analysis of three Taurus stars indicates that two, #604 and 823, are undoubtedly late-type M dwarfs, which is consistent with the results found in the previous two sections using photometric and proper motion analysis. High proper motion star #994 appears to be a background, reddened K field star. This underscores the analysis in §4 that photometric and proper

motion analysis techniques of this study are not immune to contamination by background field stars. It should be noted that the colors of #994 are not *clearly* consistent with its being a foreground M4 dwarf, but rather, are ~ 0.14 magnitudes offset from the expected values of this type of star; furthermore, the color offset is in the area of the color-color plane where the reddening curves align, making it difficult to differentiate between very late foreground stars, and reddened background objects.

These spectroscopic checks lend some confidence to the robustness of our photometric selection procedure. They also highlight the limitations of the proper motion selection criterion when used without photometric constraints. Finally, it must be emphasized that used together, the photometric and proper motion selection methods can only select *candidate* foreground objects, whose identifications must be confirmed spectroscopically.

6. The Luminosity Function

The luminosity function, $\phi(M)$, defined as the number of stars per unit magnitude interval per unit volume, is **usually** expressed in terms of either absolute visual magnitude, M_v , or absolute bolometric magnitude, m_{bol} . We adopt the former convention in this paper since it avoids additional uncertainties associated with bolometric corrections.

6.1 The Ophiuchus/Taurus I Luminosity Function

We estimate the luminosity function using the Ophiuchus and Taurus foreground candidates in Tables 1 and 3 (position coordinates given in Table 6). The two data sets are combined rather than treated separately because the volume corresponding to the Ophiuchus field, $\sim 70 \text{ pc}^3$, is too small to yield a statistically meaningful estimate of the number density of stars. The total **volume** of our Survey is $\sim 200 \text{ pc}^3$.

Expected uncertainties in ϕ arise from counting statistics, $\Delta\phi_N$, and distance estimates to the molecular clouds. The latter is given by

$$\Delta\phi_D(M_V) = 3 \left(\frac{\Delta D}{D} \right) \phi(M_V) \quad (1)$$

where D is the distance to the cloud, and ΔD is estimated distance error. Since $\Delta\phi_N$ and $\Delta\phi_D$ are

statistically independent, the total uncertainty, $\Delta\phi$, is

$$\Delta\phi = \sqrt{\Delta\phi_N^2 + \Delta\phi_D^2} . \quad (2)$$

It should be emphasized that $\Delta\phi$ represents only the internal, random uncertainties associated with the estimated luminosity function. Potentially more serious (and difficult to quantify) systematic errors are not included.

Note that the composite **Taurus + Ophiuchus luminosity function** consists of stars from different regions of the Galactic disk nearly 180° apart (though, both arc -15° from the Galactic plane). And as such, a small correction to the computed number density is required to account for the Galactic disk density gradient relative to the local solar neighborhood density. We estimate this correction using the stellar distribution model discussed in §4 (see also Jarrett 1992). The correction amounts to roughly 7% and 12% reduction in the stellar densities computed for the Taurus and Ophiuchus fields, respectively.

Our survey is incomplete in regions to the clouds. Both the Taurus and Ophiuchus data sets are limited to $V < -22.2$ mag; since the distance moduli of the clouds range from 5.7 - 6 mag, the stellar samples are complete to only $M_V < -6.4$. Consequently, the luminosity function for stars with $M_V > -16.4$ must be corrected for its lack of completeness. The usual method to correct for incompleteness is to apply the V_{\max} method (cf. Schmidt 1975). It is implemented by deducing for each star in some magnitude interval the maximum volume in **which** it can be located and still be detected in the survey. Bright stars rejected because of detector saturation limits should not affect the faint end of the foreground sample, but will limit the sample for G and K dwarfs, with $M_V < 10$; note however, that based on the Wielen et al. (1983) luminosity function, we should expect only 1 or 2 G-K dwarfs in our foreground sample.

Magnitude-limited photometric studies of the luminosity function are usually subject to Malmquist[-type] systematic bias effects in estimating stellar luminosities (cf. Stobie *et al.* 1989). We do not attempt to correct our data for these effects since **only** those **magnitude bins** with $M_V > 16$ are affected, **and** since **the** effects **are** most likely **small** compared to the **large** Poisson uncertainties that **plague** our data. Indeed, it is worth pointing out that **one** advantage of a (sufficiently) **opaque** screen **luminosity survey is its** freedom **from** Malmquist effects.

In addition to the problems of completeness that affect the faintest magnitude bins of our composite sample, there may be significant contamination from reddened field stars and/or associated

cloud members. As previously discussed in §4, we expect some level of false foreground 'detections'

the greatest source of background star contamination arises from field G and K dwarfs located some 200- 400" pc behind the clouds. Given the mean extinctions of the clouds and the limiting magnitudes of the surveys, the absolute magnitude bins affected most are those with $M_v > 15.5$ mag. From our galactic **distribution** model we estimated the degree of contamination to **the foreground** candidate sample of order 10 - 15% for the faint end of the luminosity function and roughly 10% for the bins with M_v between 9 and 11 (see Figure 5).

As a final caveat, we note that most field stars reside in binary and multiple stellar systems. Amongst the **nearby** stars, the **binary** fraction is reported to be between 30 and 50%, (cf. Henry & McCarthy 1990; Reid 1991; Fischer & Marcy 1992). Of the nearby binaries, projected separations vary from ~ 10 to 1200 a.u. (the number of stars per log separation interval is roughly constant over this range). Our survey should be sensitive to **wide binaries** (> 300 au), but is quite **incomplete beyond** 50 pc for closer pairs. We therefore expect a few binary systems within our sample to be misidentified as single star systems. The net result is that the total number density - and more important, the total mass density - will be under-represented in our survey. We shall make no corrections for stellar multiplicity, but point out that our estimate of the stellar luminosity function in fact measures the number density of stellar *systems*.

In Table 7 we show the results of binning the stars from Tables 1 and 3. The total volume surveyed is $200''$ pc³. The column denoted ϕ^* is the luminosity function adjusted according to the aforementioned effects of the Galactic density gradient and background star contamination. The number densities corresponding to magnitude bins $M_v \geq 16$ have been corrected using the V_{max} technique. Until we have further verification, we will not include the suspected dM6 star of the white dwarf- red dwarf pair (#13) in Table 7.

The composite luminosity function is shown in Figure 13. The range in values, namely $\phi_v \pm \Delta\phi_v$, is illustrated in the shaded portion of the figure. In the $M_v = 17$ bin, we show as a lower limit the uncorrected number density; the density resulting from the V_{max} correction is not shown on the plot (because it would be off-scale), but is indicated by the arrow. In spite of the substantial statistical uncertainty associated with the results shown above, the faint end of the stellar luminosity function appears to rise, or at least remain flat, beyond $M_v \sim 16$.

6.2 Discussion

in comparing this result with other determinations, we begin by noting that the the luminosity function of the nearby stars is the standard benchmark for comparison with other work in this field. In particular, the work of Wielen, Jahreiss & Kruegger (1983; hereafter referred as WJK), based on the sample of stars within 20 pc of the Sun listed in the Gliese catalogue, is the best determined luminosity function for absolute magnitudes extending to $M_v = 13 - 14$. The WJK luminosity function is plotted in Figure 13 with filled circles. Other surveys which count stars within 5.2 pc of the Sun are generally considered to be complete to absolute magnitudes much fainter than that of WJK (cf. Dahn, Liebert & Harrington 1986; hereafter referred as 111.1 I; Henry & McCarthy 1990). Though the D111 luminosity function is apparently complete to $M_v = 17$ mag, and the Henry & McCarthy K-band luminosity function is complete to the limit of the hydrogen-burning main sequence, both determinations suffer from **substantial** statistical noise the 5 pc diameter volume which they encompass is considerably smaller **than** that of the WJK study, and (here is also some concern that their samples are incomplete because of a kinematic bias toward high proper motion stars. In any event, a major advantage that the WJK, D111, and particular] y the Henry & McCarthy determinations possess is that they are sensitive to near binaries; thus, these luminosity functions represent true stellar density distributions for the solar neighborhood. Both the WJK and 111,11 functions are characterized by increasing stellar densities at faint luminosities and an apparent maximum at $M_v = 12 - 13$. Thereafter, there is a decline toward $M_v = 14$, and a general flattening of the number density at the faintest luminosities. In contrast, the K-band luminosity function determined by Henry & McCarthy exhibits a significant *rise* that extends to the luminosity limit corresponding to the lowest mass stars, at which it abruptly declines. It is interesting to note that the luminosity function of D11,11 compares quite closely with the most conservative estimate of this study, up to $M_v = 17$, while the Henry & McCarthy result is more consistent with the V_{max} -corrected results from this study.

The other major approach used to determine the stellar luminosity function is *via* photometric parallax. For reasons which are still unclear, the faint end of the luminosity function determined by this method differs significantly from that determined for the nearby stars. Photometric studies by Reid & Gilmore (1982, hereafter referred as RG; also Gilmore & Reid 1983 published a revised version of RG) and Hawkins & Bessell (1988; hereafter referred as HB) show a number density peak at $M_v = 12$ (agreeing with WJK and D111), but thereafter rapidly decline at fainter luminosities. The luminosity function of Gilmore & Reid (1983) is plotted in Figure 13 with filled squares. Both of the

RG and HB studies do suggest a rise, or at least a flattening, of the luminosity function at $M_v > 16$. However, preliminary results from a statistically significant extension of the RG survey by Tinney *et al.* (1992) seem to rule out any rise in the faint end of the luminosity function. Although the statistical errors are admittedly large, we find more stars at the faint end than these surveys do.

For comparison purposes, the large statistical errors associated with the relatively small numbers of stars in our sample can be reduced somewhat by comparing *cumulative* number densities. In table 8 we show the cumulative number of stars as a function of absolute magnitude for various luminosity functions. All the data has been normalized to the volume of this study, $\sim 200 \text{ pc}^3$, and the number densities have been summed from $M_v = 8.5$. The luminosity functions of RG and HB have also been corrected for the decreasing disk density along the Galactic poles. Also shown in the table (in parentheses) are the expected \sqrt{N} errors associated with each estimate.

It can be seen in table 8 that the cumulative number of objects **found** in this study agrees quite well with those deduced from other surveys for absolute magnitudes brighter than $M_v = 15 - 16$. **There also appears** to be good agreement between **our** results and those of DL11 for magnitudes extending to $M_v = 17$. Differences relative to the photometric parallax surveys become apparent at the fainter magnitudes. Even if we ignore completeness corrections, our study contains *more* stars at the faint end of the luminosity function where both photometric studies are presumed to be complete. The disparity is much larger if our corrected number densities are used. Other than statistical aberration, it is not clear what the cause of this apparent discrepancy is.

It has been suggested by Reid (1987; 1991; Stobie *et al.* 1989) that the differences at the faint end of the various luminosity functions arise from unresolved binary companions. Photometric parallax surveys are not sensitive to these objects. Yet simple models which factor in the contribution from various binary systems (*e.g.*, equal and unequal mass systems) imply that unresolved binaries probably cannot account for the large apparent differences between the two types of luminosity functions (see Reid 1987; 1991; Stobie *et al.* 1989). In any case, while our survey undoubtedly contains a few unresolved binary systems, they apparently cannot resolve the discrepancy between our results and the others given in table 8. We therefore tentatively conclude that the luminosity function rises beyond $M_v = 16$; even if we discard our attempts to correct for incompleteness in the faintest magnitude bins, the luminosity function at least remains flat for the lowest mass stars.

Although our statistical errors are clearly large, our provisional finding that the luminosity function again rises beyond this peak implies that *the initial mass function probably also rises for*

$M < 0.2 M_{\odot}$. This point is particularly relevant (and encouraging) to future surveys of low-mass degenerate objects, given that the IMF is usually quoted in the literature (e.g., Scalo 1986) as having a turnover for the lowest mass stars ($< 0.2 M_{\odot}$). Even if our most conservative estimate for the faint end of the luminosity function is used - in which no corrections whatsoever are made for incompleteness - we are forced to conclude that the *IMF is at least flat down to the edge of the hydrogen-burning main sequence.*

A rising IMF suggests the existence of an alternative formation mode for very low mass stars. This may be consistent with Larson's (1986; see also Larson 1992) 'bimodal' star formation mechanism, in which a second class of low mass stars forms, possibly in a burst very early in the existence of the Galaxy. Several authors (e.g. Shu, Adams & Lizano 1987; Rana 1987) have suggested a mechanism of hierarchical star formation, or multimodal bursts, each of which triggers or induces further episodes of star formation. A rising IMF that extends beyond the limit of the minimum mass required to sustain hydrogen-burning, $\sim 0.08 M_{\odot}$, would also **suggest** that there **may** be profuse numbers of degenerate "brown dwarf" objects in the **Galactic** disk. Given the absence of **any** confirmed brown dwarf candidates, however, it is difficult to avoid the conclusion that even if the IMF continues to rise for masses $< 0.08 M_{\odot}$, it must **soon** thereafter steeply decline.

Whether one chooses a flat IMF or a rising IMF (with a slope that is clearly ill-determined by this work), it should be kept in mind that any extrapolation involving brown dwarfs will possess staggering uncertainties, given our ignorance of the M-L relation and luminosity function corresponding to the brown dwarfs. Indeed, there are doubts as to the very existence of these objects. To date, there is not one firm identification of a brown dwarf or extra-solar Jupiter object. It is especially discouraging that the results from studies specifically designed to find brown dwarfs in binary and multiple stellar systems have been negative (e.g. Skrutskie 1987; Skrutskie, Forrest, & Shure 1989). What we can say definitively is that the lowest mass stars are the most common stars in the Galaxy, and that given the constraints established by our luminosity function, the *most numerous* stars in the Solar neighborhood appear to have masses very near the hydrogen-burning limit.

7. Summary

We have implemented a new method by which to study the faint end of the field star luminosity function. The method relies on deep, multicolor photometry of fields projected against highly obscured, nearby molecular clouds. The clouds act as nearly opaque screens, enabling us to delimit a well-defined survey sample volume free of the problems of distinguishing nearby, intrinsically faint dwarf stars from more distant red giants. We have demonstrated that with this technique it is possible to probe the faint end of the luminosity function out to distances much further than have been previously attempted. The main points and conclusions of this work may be summarized as follows:

- We obtained deep photographic and CCD photometry at optical (V, R, I) bandpasses towards very highly obscured portions of the Taurus and Ophiuchus molecular clouds. The fields cover a total area of ~ 0.63 square degrees, and the total volume delimited by the cloud distances is $\sim 200 \text{ pc}^3$. Within this volume, the survey is complete for all stars brighter than $M_v = 16.25$ mag; at R and I, the survey is complete down to the lowest mass stars capable of sustaining core hydrogen burning.
- Color-color criteria were used to distinguish between background, highly reddened stars and stars located in front of the clouds. The method of photometric parallax was used to deduce the absolute magnitude and spectral type of those stars found to lie in front of the clouds. We supplemented the photometry and color-color results with proper motion measurements of the candidate stars. The proper motions were obtained from our photographic and CCD data, and from the (ca. 1950) Palomar Sky Survey.
- As a test of our ability to distinguish foreground dwarfs from heavily reddened background stars, we obtained redband (6000 - 9000 Å) spectra of three Taurus stars. Two of the stars whose photometric properties led us to identify them as foreground candidates were confirmed to be late-type foreground M dwarfs, with spectral type from M5 to M6 V. The third, which was photometrically excluded as a foreground object but which had a proper motion marginally consistent with such an identification, appears to be a reddened, high velocity

background dK star. These results lend some confidence to our selection methods but prove the need to confirm the identity of each candidate star spectroscopically.

- We estimated the field star luminosity function for the composite Taurus and Ophiuchus foreground sample. We find that the faint end of the luminosity function resembles that for the *local* population as determined by Wielen *et al.* (1983) and Dahm *et al.* (1986) up to $M_v - 16$. At still fainter magnitudes, we find the shape of the luminosity function to be consistent with that exhibited by the K-band luminosity function determined by Henry & McCarthy (1991) for very low mass stars; furthermore, we find more stars than do photometric parallax studies of the polar regions. This difference widens dramatically if even the simplest correction for incompleteness is applied to our data. While statistical **noise** due to our **small Sample** size, systematic effects, the Galactic density distribution, and stellar multiplicity may all contribute to this disparity, it nonetheless seems real and substantial. Furthermore, this result is consistent with the shape of the K-band luminosity function determined by Henry & McCarthy (1990) for the lowest mass nearby stars. We therefore tentatively conclude that the luminosity function rises beyond $M_v - 16$. Even if we discard our attempts to correct for incompleteness in the faintest magnitude bins, it appears that the luminosity function at least remains **flat** for the lowest **mass** stars.
- Although our statistical errors are large, our provisional finding that the luminosity function rises again beyond its well-known peak at $M_v - 12 - 13$, also implies that the IMF probably rises beyond the turnover point associated with this **peak**. Even if our most conservative estimate for the faint end of the **luminosity** function is used - in which no corrections whatsoever are made for incompleteness - we conclude that the IMF is at least **flat** down to the edge of the hydrogen-burning main sequence.

Acknowledgments

I. I.J. thanks George Jacoby and John Salzer for their on site technical support at KPNO, and Terry Herter, Tom Greene and John Stauffer for kindly providing data. We are grateful to Dr. E. Weis for helping us obtain the single-channel KPNO photometry, and to C. Jordan for assisting with those observations. Thanks go out to Susan Kleinmann, Steve and Karen Strom, and Mike Skrutskie for many useful discussions that contributed to this work. Finally, we are indebted to Connard Dahn for a thorough review of this paper that greatly improved its focus. This research was partly supported by a Grant-in-Aid of Research from Sigma Xi, The Scientific Research Society, NSF grant AST89 to the University of Massachusetts, and by NASA grants made under the IRAS guest investigator program. This work was also carried out in part at the Jet Propulsion Laboratory, California Institute of Technology, under a contract with the National Aeronautics and **Space** Administration. R.L.D's **work in no way** represents the **views of** the National Science Foundation.

Appendix Proper Motion Measurements

To carry out the proper motion analysis, we obtained digitized images of the Taurus and Ophiuchus regions from glass plate copies of the National Geographic Palomar Observatory Sky Survey (1'0SS) at the National Optical Astronomy Observatories in Tucson, Arizona. Since the object fields are all heavily obscured, the red (E)-plates of the survey were used to minimize the molecular cloud extinctions. The plates used were: E-228 Taurus epoch 1950.9 and E-1105 Ophiuchus epoch 1954.5. Stars within a 1.5° square area centered on the clouds were identified and their relative magnitudes computed using the "Monet Machine" automatic measuring engine. The result was a catalog of several thousand stars within the Taurus and Ophiuchus fields, with cartesian coordinates and machine magnitudes.

The accuracy of the coordinates obtained in this way depends in part upon the actual location of the stellar images on the glass plate. Distortion due to buckling of the glass as it is placed in the plate holder of the telescope typically amounts to $(0.5'' - 1.3''$; for the most part, less than a $1''$ position error can be expected (*cf.* Bowen 1960). The relative brightnesses of the scanned stellar images are accurate to ~ 0.5 magnitudes, which is adequate for our purposes, but there is a non-linear relation between actual and machine magnitudes (Jarrett 1997.). Since our goal was to extract all stars on the plates brighter than the plate limit ($R_{\text{lim}} \sim 20$; Minkowski & Abell 1963), the machine was set to an extreme brightness threshold. Unfortunately, this choice also resulted in the unavoidable side effect of numerous false detections. For the most part, these pseudo-stars were easily culled using a magnitude criterion, as their apparent brightness is typically very low.

The general technique that we use to determine proper motions is to compare our 4-m photographic data and data from the red 1'0SS plates with our corresponding CCD data. The field pairs used in the calculation of the stellar proper motions are:

CCD R-image vs. POSS E-plate; Taurus baseline = 39.0 years, Ophiuchus = 35.9 years, and
 CCD I-image vs. 4m N-band photographic plate; Taurus = **3.1 years** and Ophiuchus = 8.0 years.

Our approach is to use a set of reference stars to define a positional mapping between two data sets. The fitted fields **must** be kept **small** in order to keep the transformation fit **as accurate as possible**; this is especially crucial in the case of POSS data, since the physical curvature of the

Schmidt plate during exposure introduces appreciable large-scale field distortions. The functional form of the mapping adopted here is a cubic polynomial, which we fit with the aid of a least squares analysis. The reference stars chosen for the fit must exhibit negligible angular shift (consequently, most will be field stars, located far from the Sun), and they must as far as possible be uniformly distributed relative to each other (otherwise, the cubic polynomial will be biased for those stars closely grouped together). Note also that the reference stars have colors that are comparable to any foreground stars due to the reddening effect of the molecular cloud. The relative positions are then further refined by fitting a linear polynomial to the *local* group of stars immediately surrounding each star. The set of local reference stars is, as far as possible, confined to a rectangular area typically only 5-10 arc minutes in diameter. The use of such local mappings in the vicinity of each candidate star maximizes the accuracy of any angular shifts. With this technique we expect the positional uncertainties to be in the range of 1 - 2'' cent⁻¹. The photographic data generally have greater positional accuracy than the CCD data because the centroid computations are limited by only the size of the emulsion grains themselves (size - several microns). The robustness of our technique is demonstrated by our ability to recover easily the proper motions of the Jones & Herbig (1979) sample of stars toward Taurus. Further details are provided in Jarrett (1992).

Taurus Photometric Foreground Candidates

ID#	V (A)	V-R (A)	R-I (A)	M_v	M_v	M_v	d (pc)	d_0 (pc)	d_+ (pc)	$\mu_\alpha \cos \delta$ "cent ⁻¹	μ_δ "cent ⁻¹	$\Delta\mu$ "cent ⁻¹
18	18.78 (0.07)	1.43 (0.06)	1.72 (0.04)	13.15	13.49	13.97	71	113	155	3.4	-1.0	0.8
291	17.85 (0.07)	1.21 (0.05)	1.55 (0.03)	11.81	12.04	12.35	111	145	179	-1.9	-7.4	0.8
241	17.68 (0.07)	1.24 (0.05)	1.49 (0.03)	11.64	11.87	12.16	112	145	179	6.2	-5.4	0.8
604	20.53 (0.08)	1.55 (0.07)	1.99 (0.04)	14.68	15.08	15.48	66	123	180	-4.9	-6.4	1.0
794	21.33 (0.14)	1.78 (0.12)	2.04 (0.05)	15.48	16.10	16.66	60	111	163	4.6	-3.3	0.8
823	21.15 (0.11)	1.89 (0.09)	2.15 (0.05)	16.32	16.73	17.03	41	77	112	0.4	3.8	0.8
926	15.61 (0.01)	1.07 (0.01)	1.08 (0.01)	10.00	10.04	10.08	100	130	160	1.6	-0.8	0.8
948	21.60 (0.13)	1.63 (0.11)	2.01 (0.05)	14.84	15.48	16.02	90	167	245	0.9	3.8	0.8
984	21.61 (0.14)	1.57 (0.12)	1.88 (0.05)	14.05	14.76	15.40	125	234	343
1235 ^a	15.37 (0.01)	1.07 (0.02)	1.31 (0.03)	10.68	10.81	10.95	63	82	100	5.0	-4.0	1.0
1433 ^b	16.30 (0.06)	1.01 (0.05)	1.07 (0.02)	9.72	9.92	10.08	138	189	233	-0.4	-0.8	1.0
5017 ^a	14.29 (0.01)	1.15 (0.01)	1.46 (0.01)	11.48	11.54	11.59	27	36	44	8.3	-7.2	1.3

Table notes: (a) secondary photometric standard; (b) possible double: located within $-9''$ of a faint red star.

TABLE 2

Taurus Stars with Anomalous Colors

ID#	V (A)	V-R (A)	R-I (A)	$\mu_{\alpha} \cos \delta$	μ_{δ}	$\Delta\mu$
				"cent ⁻¹	"cent ⁻¹	"cent ⁻¹
626	21.78 (0.16)	0.70 (0.12)	1.41 (0.12)
1136	21.15 (0.17)	0.35 (0.13)	1.30 (0.11)
1543	21.88 (0.22)	0.98 (0.17)	1.84 (0.13)
90"	21.90 (0.16)	1.06 (0.13)	1.88 (0.09)	29.	36.	1.3
893	22.08 (0.19)	1.77 (0.17)	2.52 (0.07)
32	21.87 (0.14)	2.31 (0.11)	2.63 (0.06)	0.7	2.3	1.3
847	20.61 (0.12)	2.55 (0.09)	2.52 (0.05)	-0.5	-0.5	1.3
1004	20.96 (0.14)	2.38 (0.11)	2.32 (0.05)	0.7	0.3	1.8

Table notes: (a) measured proper motion is not **reliable** due to faint **R-band** magnitude of star

TABLE 3

Ophiuchus Photometric Foreground Candidates

ID#	V (A)	V-R (A)	R-I (A)	M_v	M_0	M_v	M_v	(PC)	d (pc)	d_0 (PC)	d. (PC)	$\mu_\alpha \cos \delta$ "cent ⁻¹	μ_δ "cent ⁻¹	$\Delta\mu$ "cent ⁻¹
5	21.68 (0.14)	1.68(0.12)	1.98 (0.05)	14.92	15.56	16.17			90	167	245	-1.1	6.3	2.5
19	21.25 (0.11)	1.51 (0.09)	1.87 (0.05)	13.90	14.45	15.00			123	230	336	2.2	-5.0	1.3
43	17.40 (0.07)	1.30 (0.06)	1.61 (0.04)	12.22	12.60	12.94			70	91	112	-5.5	7.5	1.3
74	21.87 (0.14)	1.86 (0.12)	2.18 (0.06)	16.17	16.66	17.09			59	110	161	1.1	1.1	1.3
92 ^a	16.61 (0.07)	1.13 (0.04)	1.60 (0.03)	11.81	12.04	12.28			63	82	101	-1.1	3.8	1.3
103 ^b	20.28(0.09)	1.41 (0.07)	1.72(0.04)	13.01	13.44	13.90			147	233	319	1.1	3.8	1.3
218	22.15 (0.17)	2.01(0.14)	2.31 (0.06)	16.85	17.24	17.51			51	96	141	-6.5	-1.3	2.1
220	22.04 (0.15)	1.51 (0.13)	1.95 (0.06)	14.05	14.76	15.48			152	285	418	-1.1	7.5	1.3
221	22.11 (0.16)	1.92 (0.14)	2.30 (0.06)	16.60	17.03	17.41			55	104	152	4.3	11.3	2.1
587 ^a	11.99 (0.02)	0.62 (0.02)	0.54 (0.02)	6.74	6.91	7.07			80	104	128	10.8	-5.0	3.8
777 ^a	10.88 (0.02)	0.56(0.02)	0.48 (0.02)	6.19	6.38	6.56			61	80	98	1.1	-0.8	2.1

Table notes: (a) secondary photometric standard; (b) partially resolved double or young stellar object.

TABLE 4

Taurus Foreground Candidates **based on R,I Analysis**

ID#	l	R-1	(A)	M _r	σ_{M_r}	μ_{M_r}	d (pc)	d_0 (pc)	d ₁ (pc)	A _v	Type	d(pc)
1859	18.36	2.39	(0.06)	13.3	13.6	13.9	78	89	101	4.1	M4 V	170
2105	18.56	2.31	(0.07)	12.9	13.2	13.6	100	116	136	9.5	G3 V	600
2147	18.16	2.29	(0.05)	12.9	13.1	13.4	90	101	113	3.6	M4 V	175
2228	18.04	2.19	(0.04)	12.5	12.7	12.9	110	120	130	7.1	KS V	420
2262	19.06	2.33	(0.11)	12.8	13.3	13.9	110	140	178	9.8	F5 v	1600
2347	18.00	2.13	(0.04)	12.2	12.4	12.6	120	133	145	8.5	G3 V	600
2387	18.22	2.23	(0.05)	12.0	12.9	13.1	100	119	130	8.3	F8 v	1300
2411	18.51	2.24	(0.06)	12.6	12.9	13.2	116	130	153	7.5	G8 v	840
2429	18.61	2.25	(0.07)	12.6	13.0	13.3	116	136	160	0.4	A0 V	1800
2430	18.57	2.31	(0.07)	12.9	13.2	13.6	100	120	136	10.4	A3 V	1500
2532	18.10	2.37	(0.06)	13.3	13.5	13.8	75	82	92	12.2

TABLE 5

Ophiuchus Foreground Candidates based on R,J Analysis

ID#	1	R-1	(A)	M _r	₀ M ₁	_r M ₁	(l. (pc)	d ₀ (pc)	d _r (pc)	A _v
-397	18.03	2.30	(0.07)	12.9	13.2	13.5	105	123	143	11.2
398	18.79	2.39	(0.08)	1.2	13.0	14.0	91	108	129	11.2
450	18.70	2.39	(0.08)	13.2	13.6	14.0	87	104	124	13.3
465	18.55	2.29	(0.06)	12.9	13.1	13.4	100	121	140	11.1
466	18.43	2.25	(0.06)	12.7	13.0	13.2	109	125	143	11.4

TABLE 6

Taurus and Ophiuchus Coordinate Positions

Taurus			Ophiuchus		
ID#	RA(1950)	DEC(1950)	ID#	RA(1950)	DEC(1950)
18	4:38:24.9	25:26:37	5	16:29:05.1	-24:34:09
29	4:38:38.2	25:28:30	19	16:30:08.3	-24:32:10
241	4:37:27.5	25:38:08	43	16:30:00.0	-24:24:05
604	4:38:17.1	25:47:02	74	16:30:01.9	-24:21:26
794	4:36:20.4	25:33:54	92	16:29:33.6	-24:17:32
823	4:36:32.1	25:36:54	103	16:29:35.2	-24:16:38
926	4:37:15.4	25:45:14	113	16:29:31.3	-24:16:03
948	4:35:44.7	25:46:28	218	16:29:59.0	-24:23:55
984	4:37:01.5	25:48:35	220	16:29:27.1	-24:32:57
994	4:37:33.8	25:49:12	221	16:30:08.7"	-24:21:14
1235	4:38:37.5	25:58:06	587	16:29:07.8	-24:16:40
1433	4:38:24.2	26:03:39	777	16:29:21.0	-24:33:51
5017	4:37:03.0	25:30:58

TABLE 7

The Combined Taurus and Oph 1 luminosity Function

M_v		$\phi(M_v)$	$\phi^*(M_v)$
(± 0.5)	N	(100 x stars mag ⁻¹ pc ⁻³)	
9	1	0.5 (0.5)	0.5 (0.5)
10	2	1.0 (0.7)	0.8 (0.7)
11	1	0.5 (0.5)	0.5 (0.5)
12	4	2.0 (1.0)	1.8 (1.1)
13	3	1.5 (0.9)	1.3 (1.0)
14	3	1.5 (0.9)	1.3 (0.9)
15	3	1.5 (0.9)	1.3 (0.9)
16	1	0.5 (0.5)	0.4 (0.5)
17	4	2.0 (1.0)	11.5 (6.8)
18	<1	< 0.5 (0.5)	< 9.0 (4.0)

Table Notes: ϕ_v is the uncorrected **number** density, and the **values** in parenthesis the corresponding \sqrt{N} uncertainty; ϕ^*_v is the **number density** corrected for completeness, the Galactic density **gradient** and **background** star contamination, and the **values** in parenthesis the corresponding total uncertainty.

TABLE 8

Cumulative Number of Objects from Various Surveys

M_V^{lim}	this study ^a	N_V^{lim}					
		WJK	DLH	GR	HB ^b	NGP ^c	
9.5	1 (1)	1 (1)	1 (1)	1 (1)	1 (1)	1 (1)	
10.5	3 (2)	2 (1)	2 (1)	2 (1)	2 (1)	2 (1)	
11.5	4 (2)	4 (2)	3 (1)	4 (2)	4 (2)	4 (2)	
12.5	7 (3)	7 (2)	6 (2)	8 (3)	7 (2)	6 (2)	
13.5	10 (3)	11 (3)	9 (3)	10 (3)	9 (3)	8 (3)	
14.5	12 (4)	14 (4)	10 (3)	12 (3)	10 (3)	9 (3)	
15.5	15 (4)	16 (4)	14 (4)	12 (3)	11 (3)	10 (3)	
16.5	16 (4)	17 (4)	16 (4)	13 (3)	12 (3)	10 (3)	
17.5	>19 (4)	39 (6)	18 (4)	18 (4)	13 (3)	12 (3)	11 (3)
18.5	--	--	18 (4)	...	14 (3)	12 (3)	...

Table Notes: (a) The value corresponding to $M_V = 17.5$ represent lower limits in the left hand box; the right hand boxes contain the value corrected by the V_{max} technique. (b) Corrected to the local number density (taken from Fig. 5 in Stobie *et al.* 1989). (c) Determined for stars toward the NGP (Stobie *et al.* 1989).

List of Figures

Figure 1 Visual extinction map of the Heiles' Cloud 2 CCD field. The map is based on star counts in a grid of 41×37 rescau cells, each $1.4'$ square. Contour levels correspond to $A_V = 5$ and 10 msg. The A_V grey-scale values range from 3 to 23 mag (white to black).

Figure 2 Visual extinction map of the Ophiuchus CCD field. The map was constructed from star counts in a grid of 21×19 rescau cells, each $1.25'$ square. Contour levels correspond to $A_V = 5$ and 10 msg. The A_V grey-scale values range from 3 to 21 mag (white to black).

Figure 3 Model predictions of the absolute magnitude histogram of the stars located within a $1^\circ \times 10$ area in the direction of the Taurus molecular cloud ($Q = 173^\circ$, $b = 13.60$). In case (a), $A_V^{\text{cloud}} = 0$ is assumed, *i.e.*, there is no obscuration due to the cloud; in case (b), the cloud, located at a distance of 140 pc, functions as a dark screen. The solid line represents dwarf stars, the dotted line evolved disk giants, and the dot-dashed line spheroidal stars.

Figure 4 CCD photometry of the Taurus sample, presented in the (V-R) vs. (R-I) plane. The V-band 10% and 20% limiting magnitudes are roughly 21.2 and 22.0, respectively. Stars with visual magnitudes brighter than 13 arc excluded. Color uncertainties, represented by 1σ error bars, are also shown; stars with $\Delta(R-I) > 10\%$ arc excluded. All stars are located along a line of sight with at least 3 magnitudes of visual extinction. Mean colors of main-sequence G - M dwarfs are represented by the solid line, and giants by the dashed line (Bessell 1991; Johnson 1966).

Figure 5 Model predictions of detection frequency of foreground stars and background contaminant stars. The values are computed using the opaque screen method and the stellar distribution model described in the text. Foreground candidates ("detections") must satisfy the following two conditions: (1) VRI colors such that $\zeta < \zeta_{\text{max}}$, where ζ is the minimum difference in magnitude between the stellar colors (V-R) & (R-I) and the corresponding main-sequence color, (V-I₀ & (R-I)), and (2) photometric parallaxes $d < d_{\text{cloud}}$. In case (a), $A_V^{\text{cloud}} = 0$; in case (b), the cloud functions as a dark screen. The solid line represents

the ratio of stars detected as foreground objects relative to the 'true' total foreground stars. The dashed line corresponds to the ratio of background stars (with false foreground detections) relative to the total foreground candidate sample (including true and false foreground detections).

Figure 6 CCD photometry of the Taurus candidate foreground stars presented in the (V-R) vs. (R-I) plane. These stars (denoted by filled circles) have colors that lie within ± 0.1 mag (dashed lines) of the main sequence track (solid line), and have a photometric parallax placing them in front of the molecular cloud ($d < 140$ pc). Also plotted (filled triangles) are the colors of visual doubles, triples, or stars with extended structure. The remaining stars in the sample (see Figure 4) are plotted with small dots.

Figure 7 CCD photometry of the Ophiuchus sample, presented in the (V-R) vs. (R-I) plane. The V-band 20% limiting magnitude is -22.2 . Stars with visual magnitudes brighter than 12 are excluded. Color uncertainties, represented by 1σ error bars, are also shown; stars with $\Delta(R-I) > 1$ mag are excluded. All stars are located along a line of sight with at least 3 magnitudes of visual extinction. As with Figure 6, mean colors of main-sequence G - M dwarfs are represented by the solid line, and giants by the dashed line.

Figure 8 CCD photometry of the Ophiuchus candidate foreground stars presented in the (V-R) vs. (R-I) plane (denoted by filled circles). See Figure 6 for a description of the remaining symbols.

Figure 9 Spectrum of Gl. 406. This dwarf star is of spectral type M6 V.

Figure 10 Spectrum of candidate foreground star #604. The flux levels are in units of 10^{-16} ergs $\text{cm}^{-2} \text{sec}^{-1} \text{\AA}^{-1}$.

Figure 11 Spectrum of candidate foreground star #823. The flux levels are in units of 10^{-16} ergs $\text{cm}^{-2} \text{sec}^{-1} \text{\AA}^{-1}$.

Figure 12 Spectrum of high proper motion star #994. The flux levels are in units of 10^{-15} ergs cm^{-2} sec^{-1} \AA^{-1} .

Figure 13 The combined luminosity function (in units of stars pc^{-3} mag^{-1} $\times 10^4$) for the Taurus and Ophiuchus fields. The range in density, $\phi_V \pm \Delta\phi_V$, is illustrated with grey shaded magnitude bins. The values have been corrected for the Galactic density gradient and contamination from background stars. Due to completeness problems, the $M_V = -17$ bin value represents a lower limit to the true density; the density resulting from the V_{max} correction is not shown on the plot (due to a dynamic range constraint), but is indicated by the arrow. Also shown are the observed luminosity functions of Wielen, Jahreiss & Krucgger (1983; denoted by filled circles), and Gilmore & Reid (1983; denoted by filled squares), where the error bars correspond to the \sqrt{N} uncertainty in each bin.

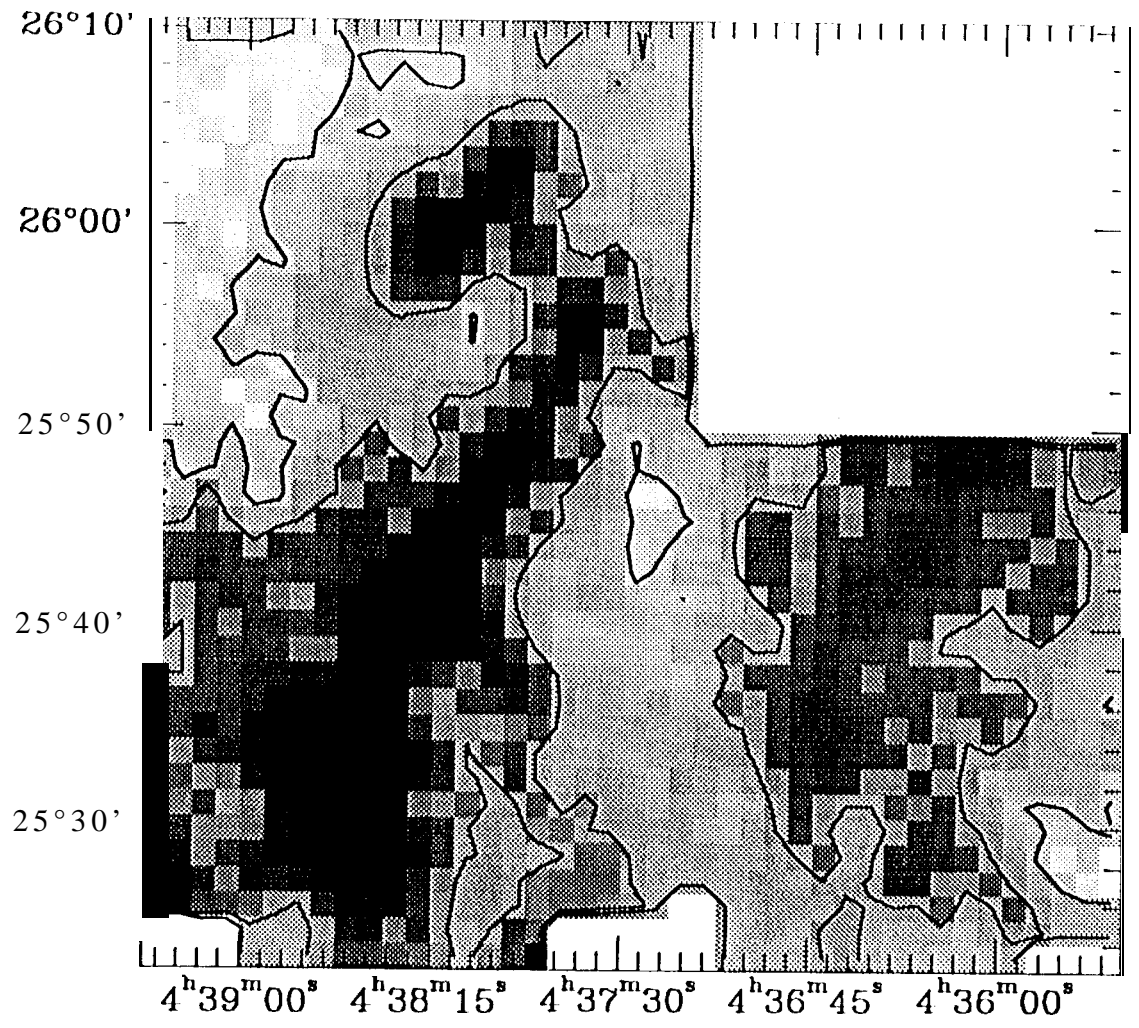


Fig 1

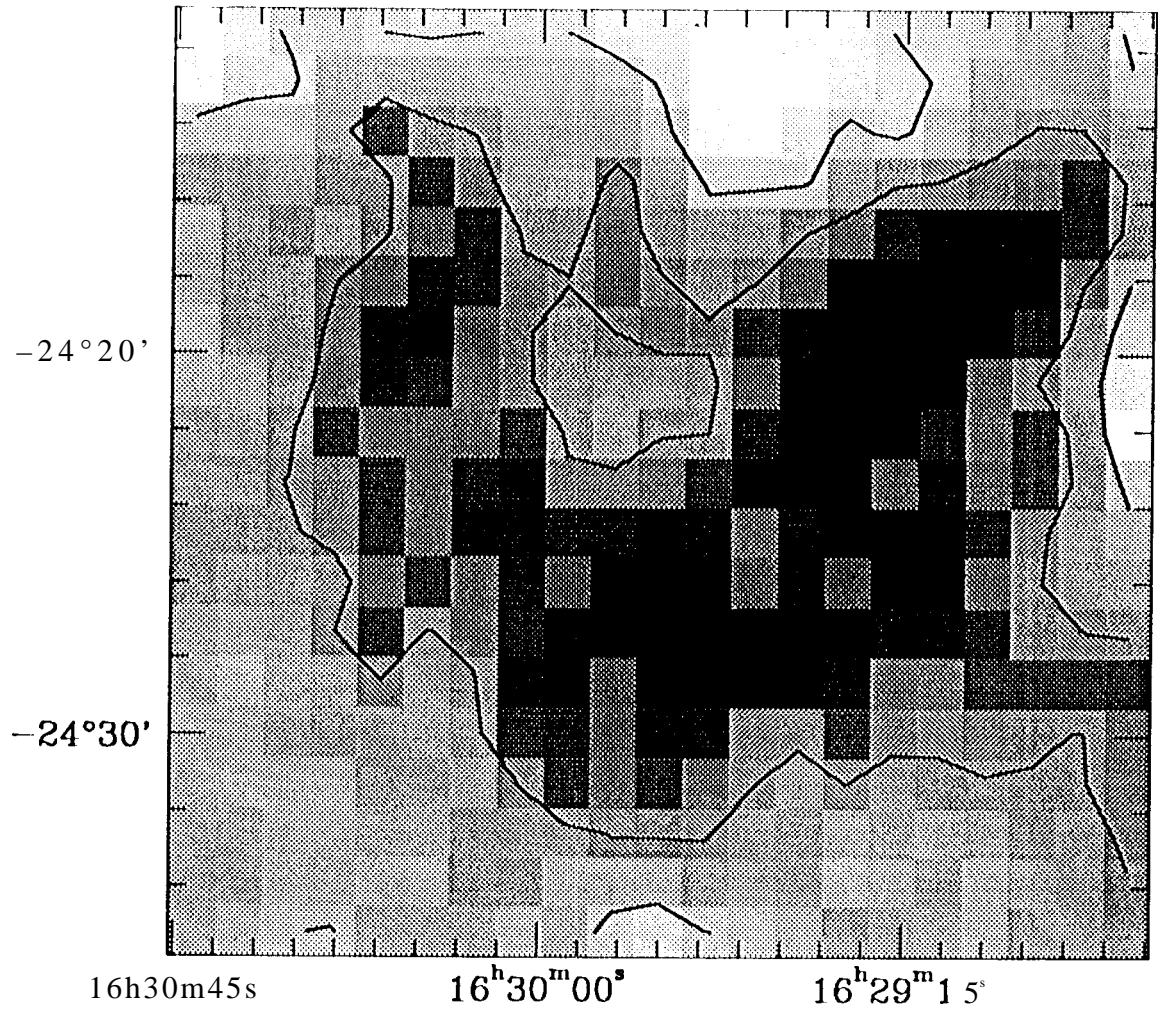


Fig. 1

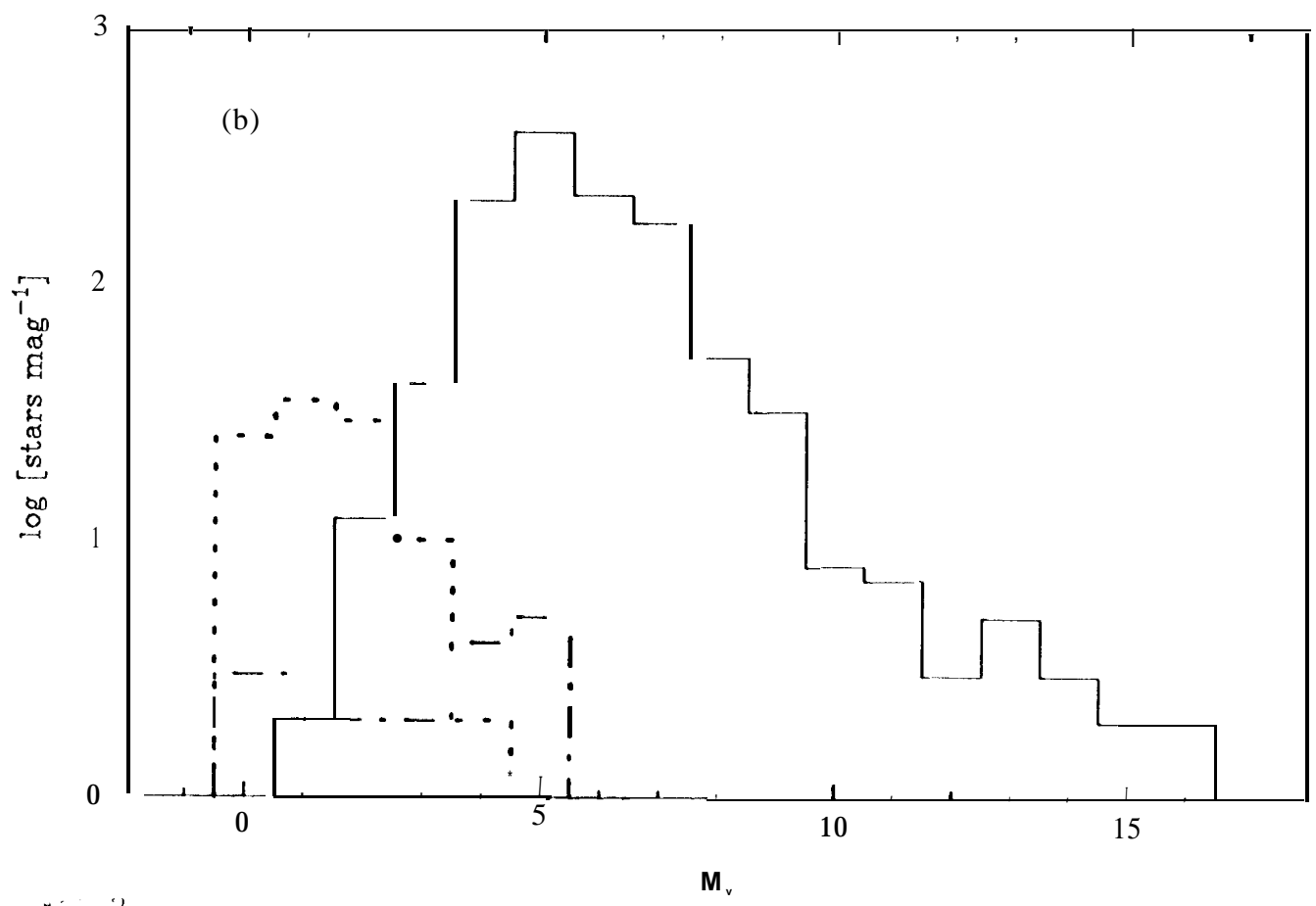
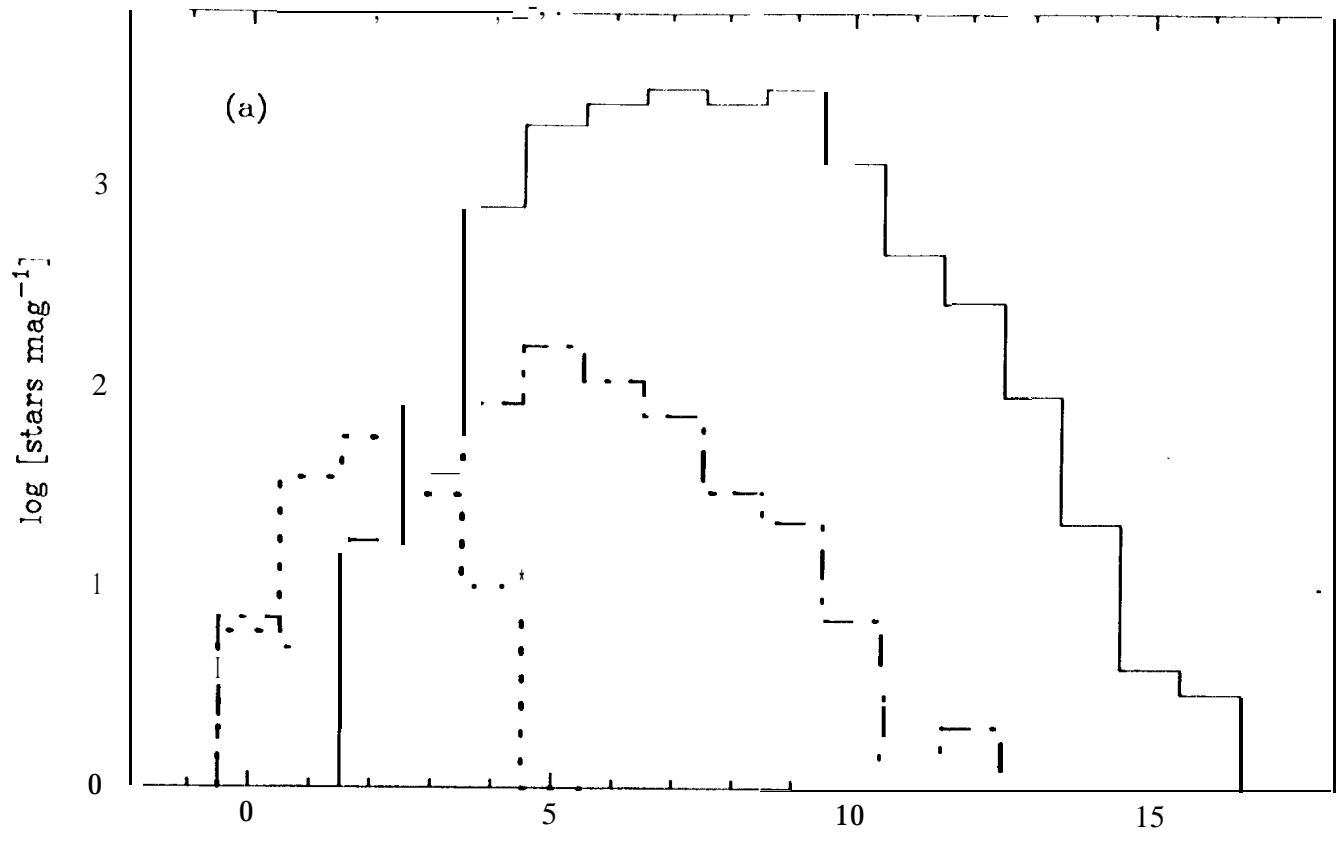


Fig 3

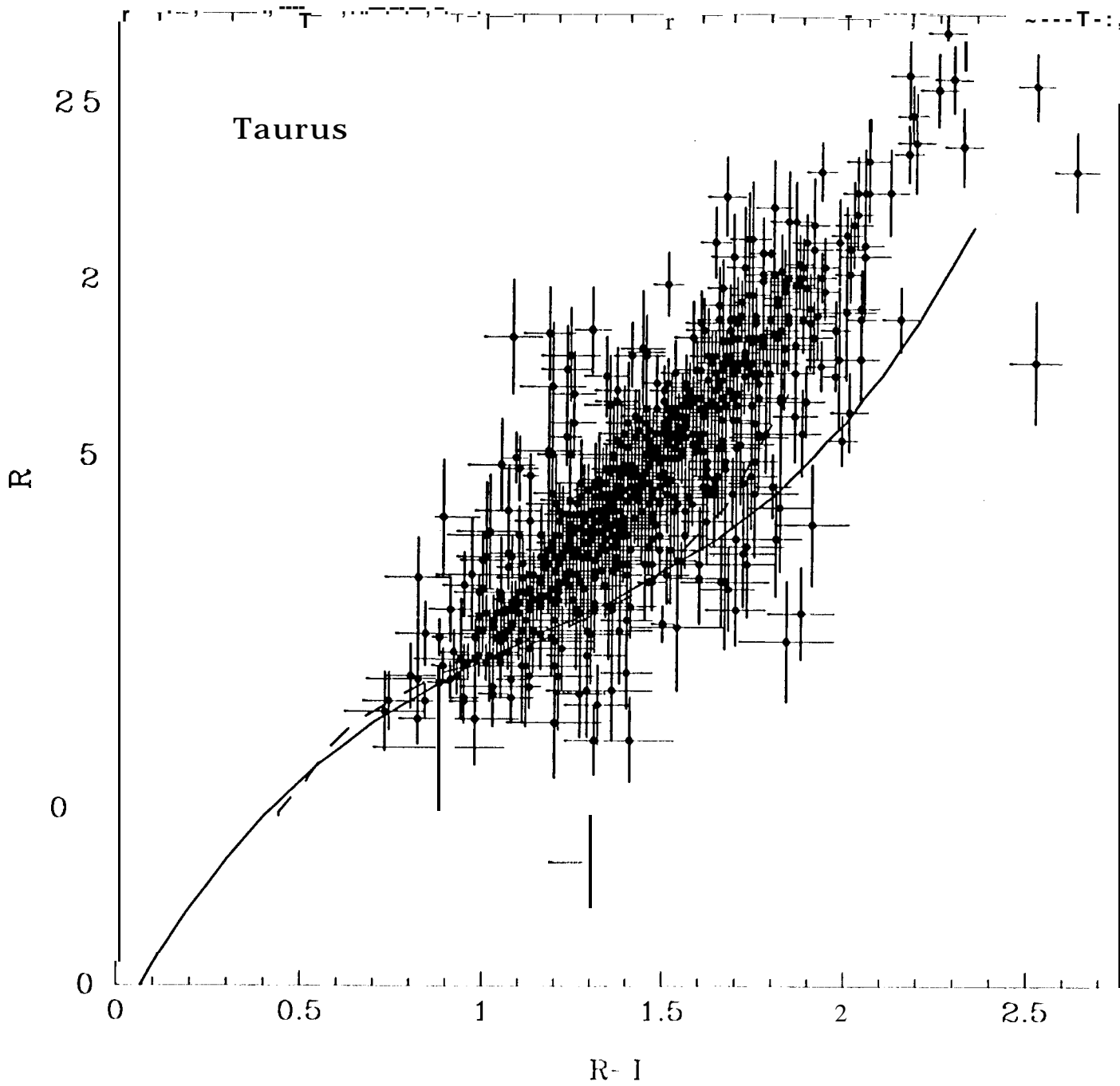
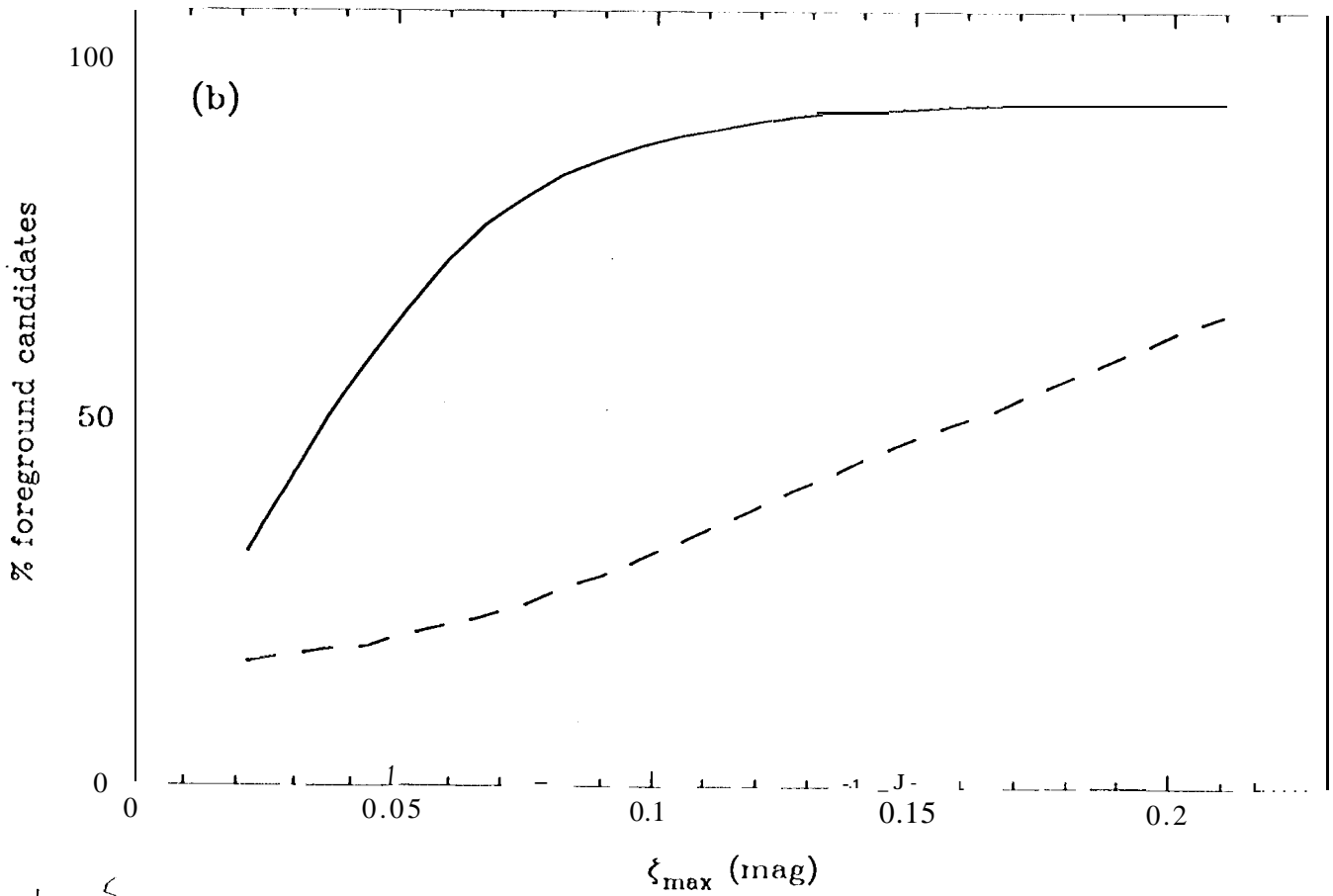
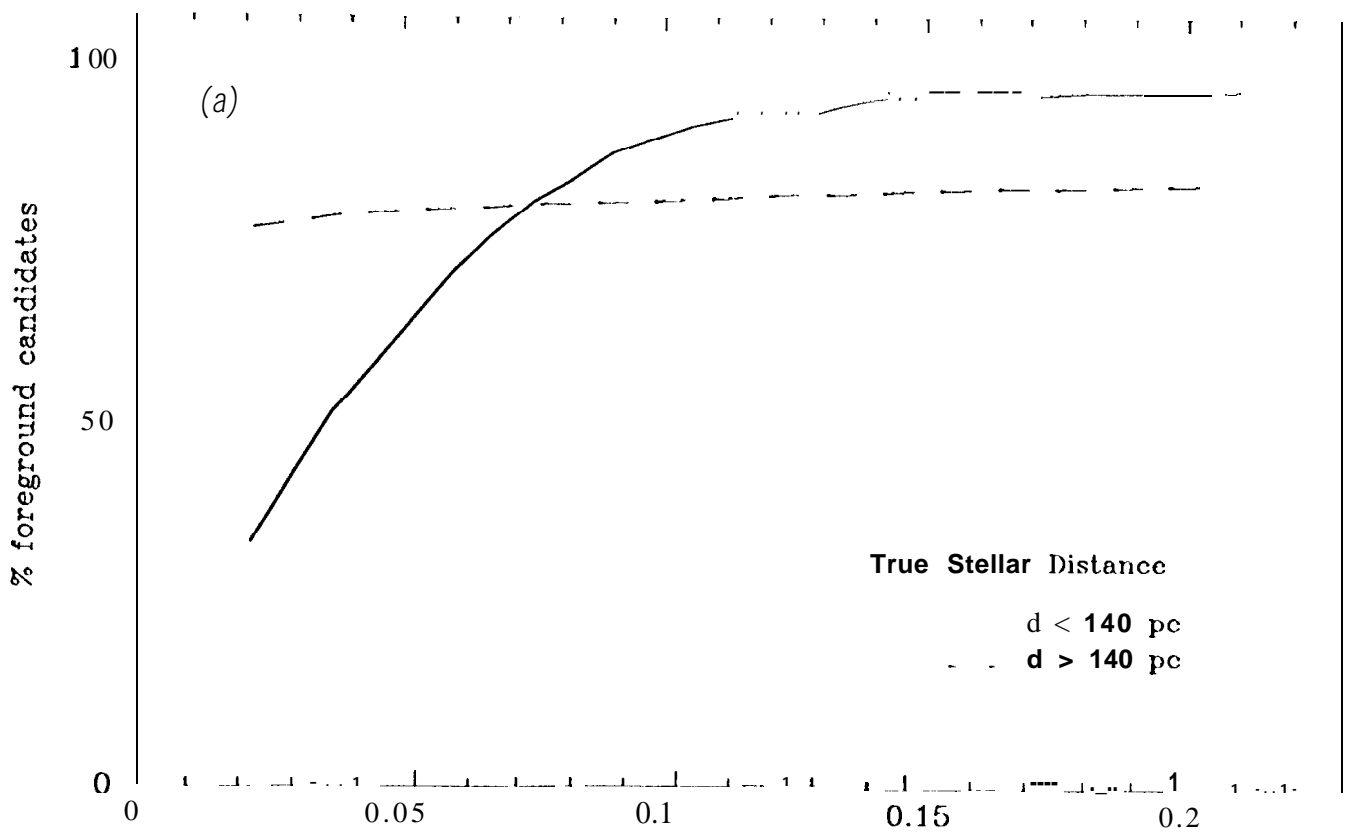


Fig 4



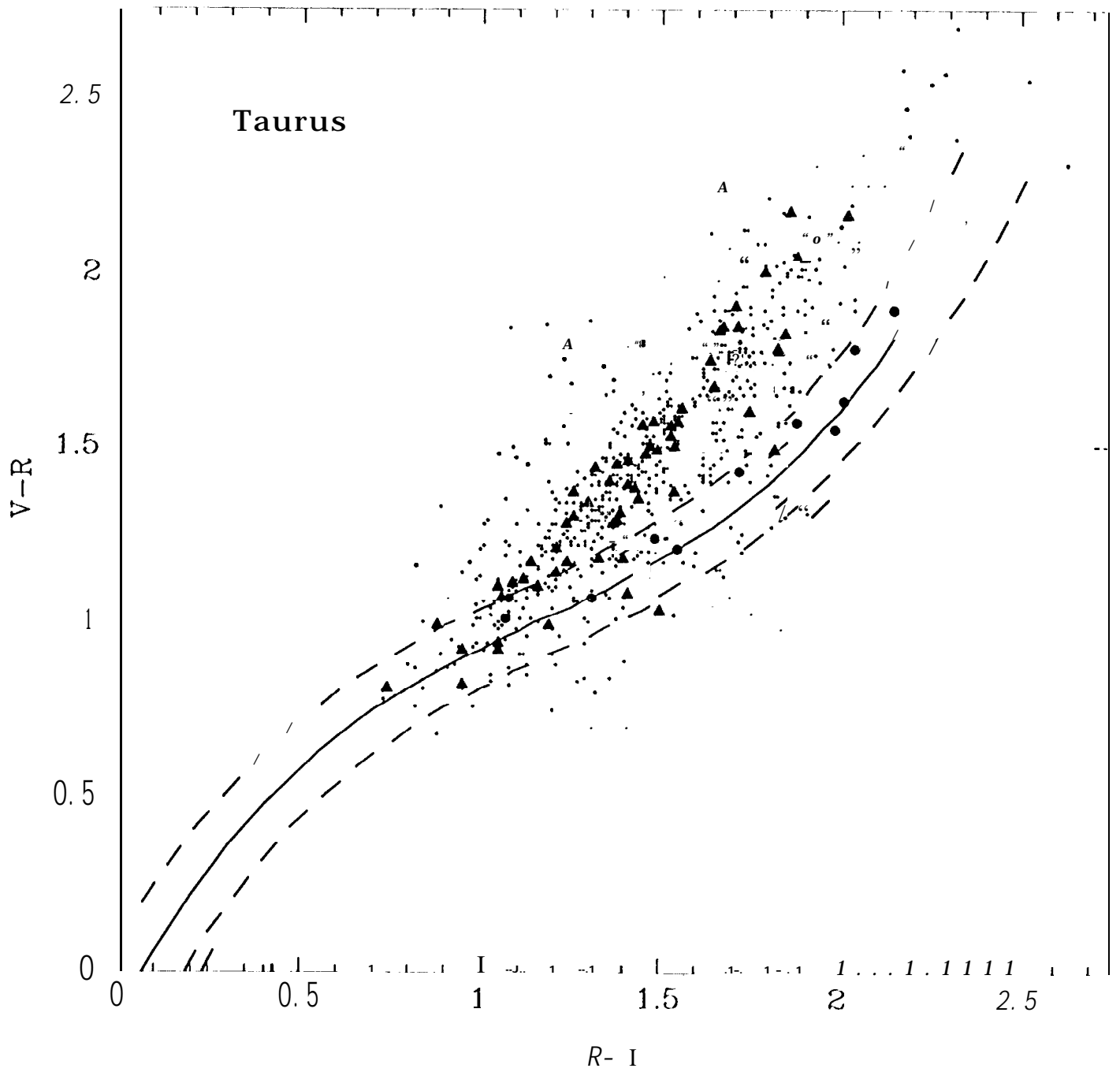


Fig 6

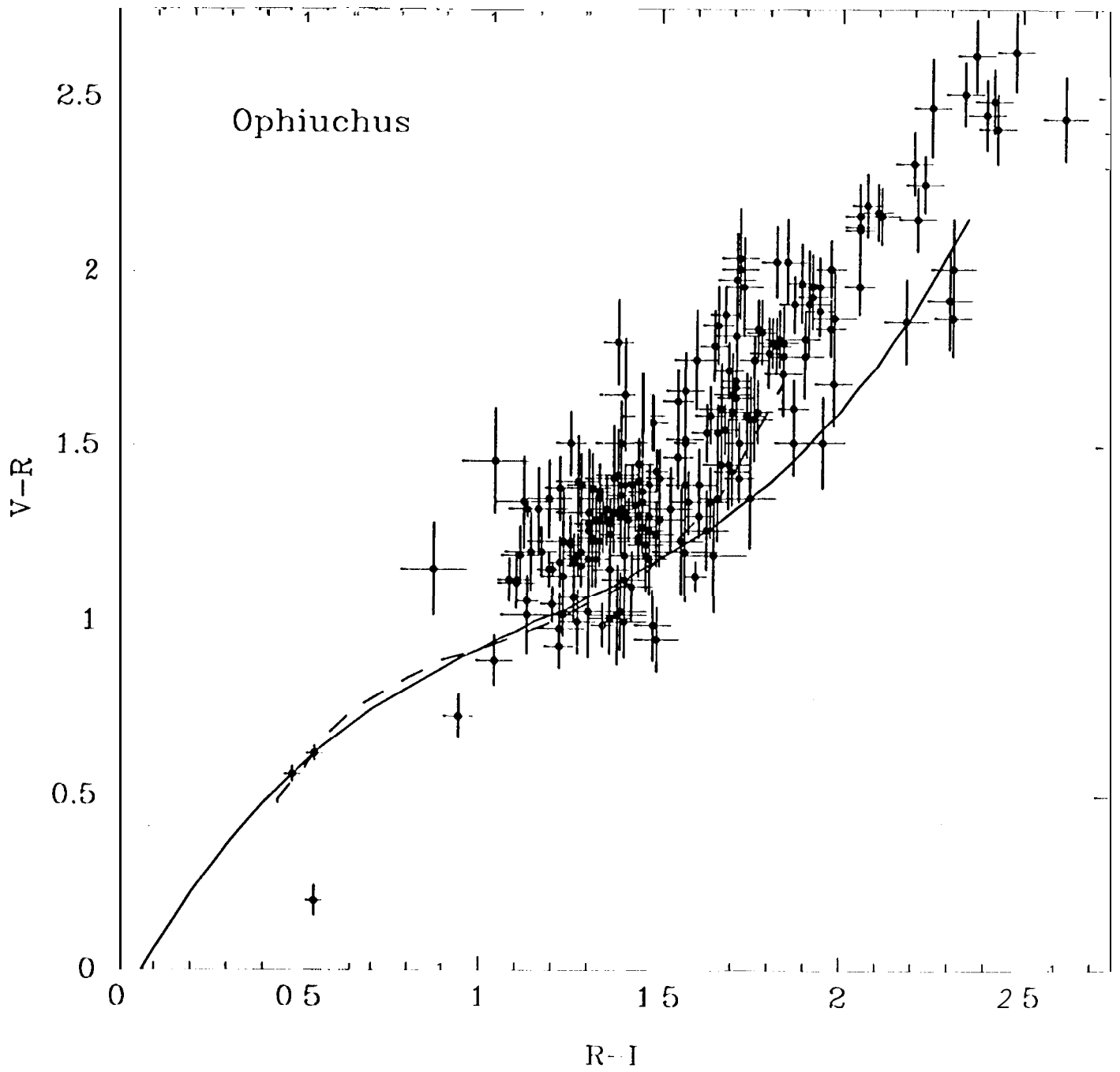


Fig 7

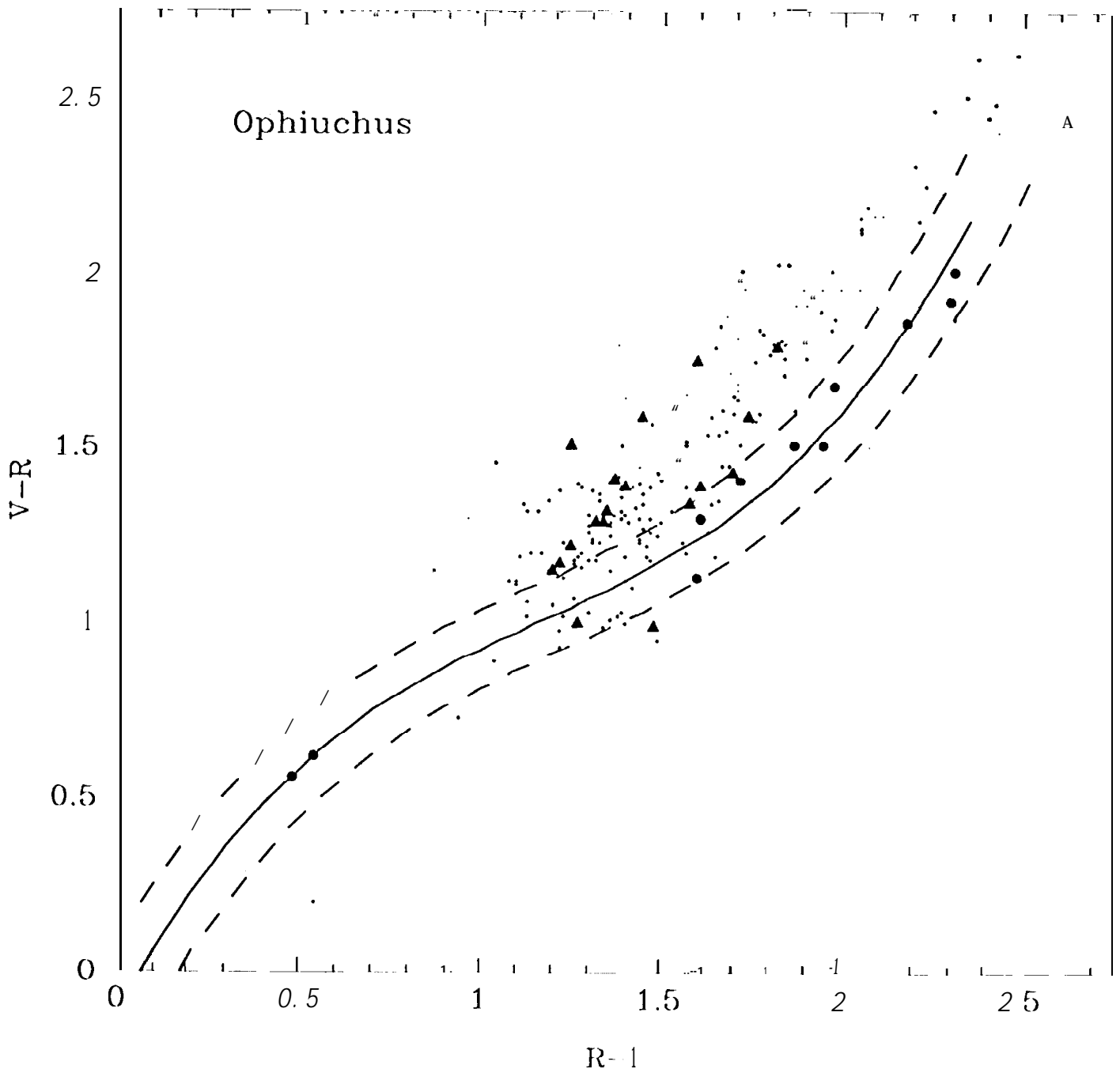


Fig 8

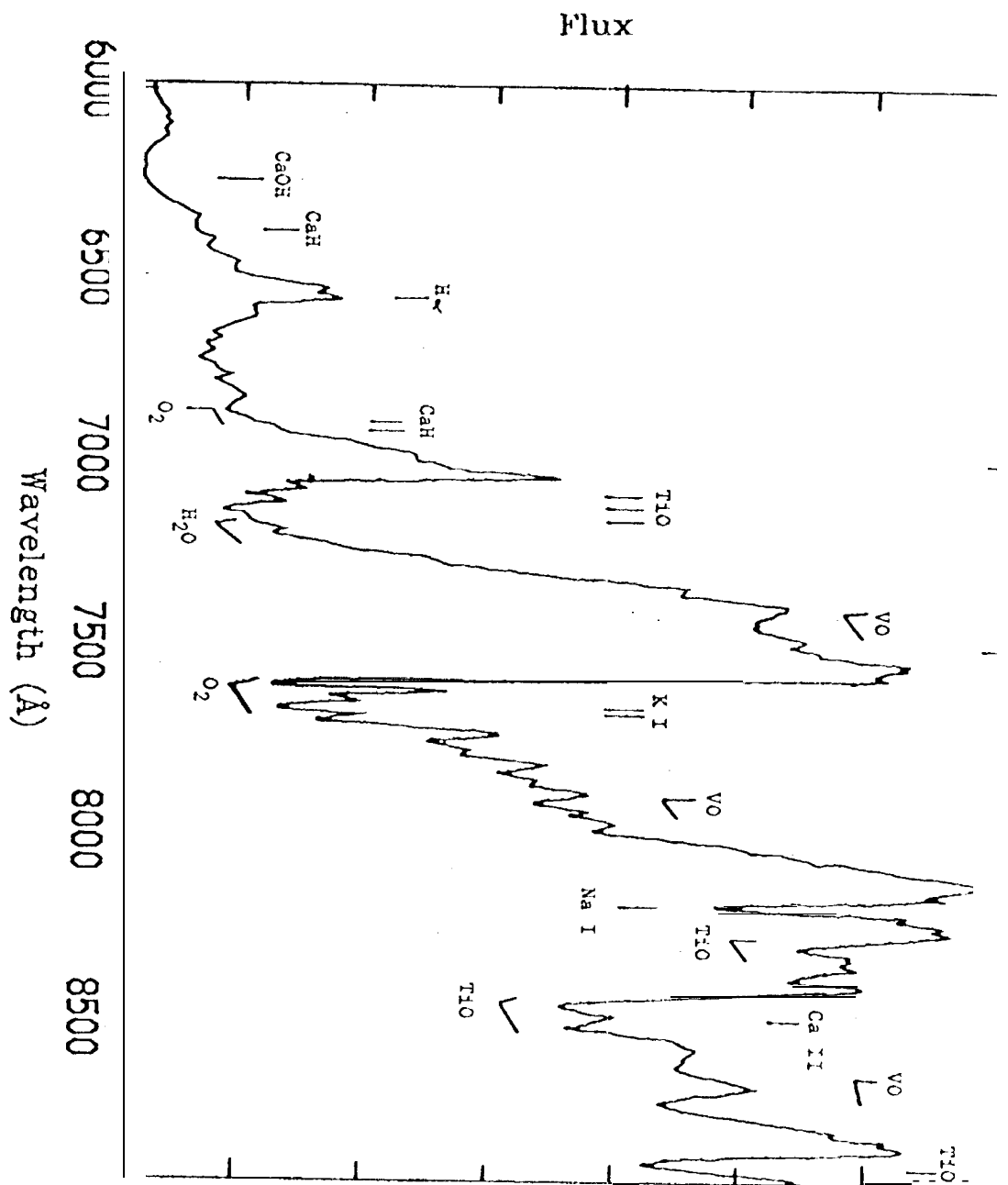
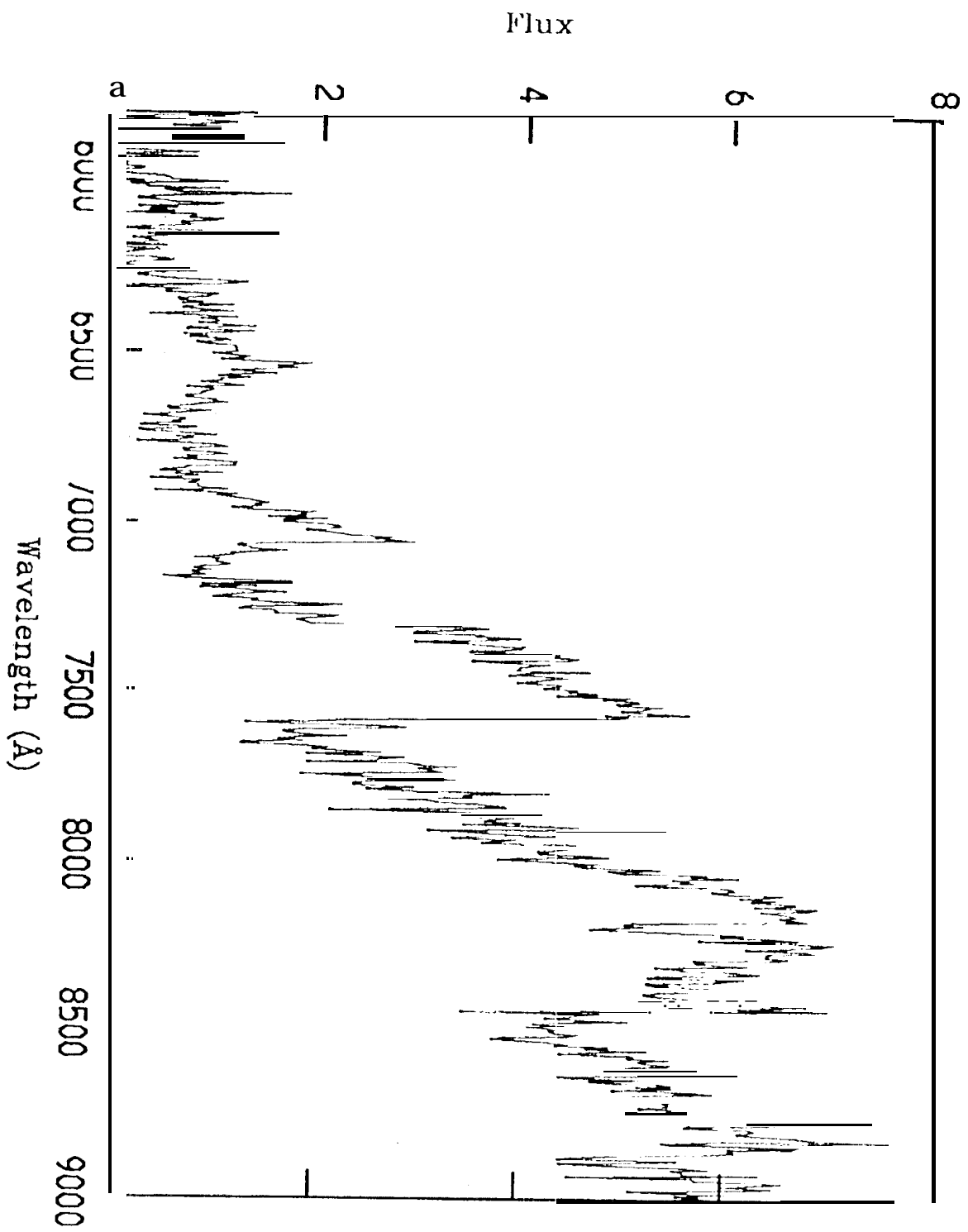


Fig. 9



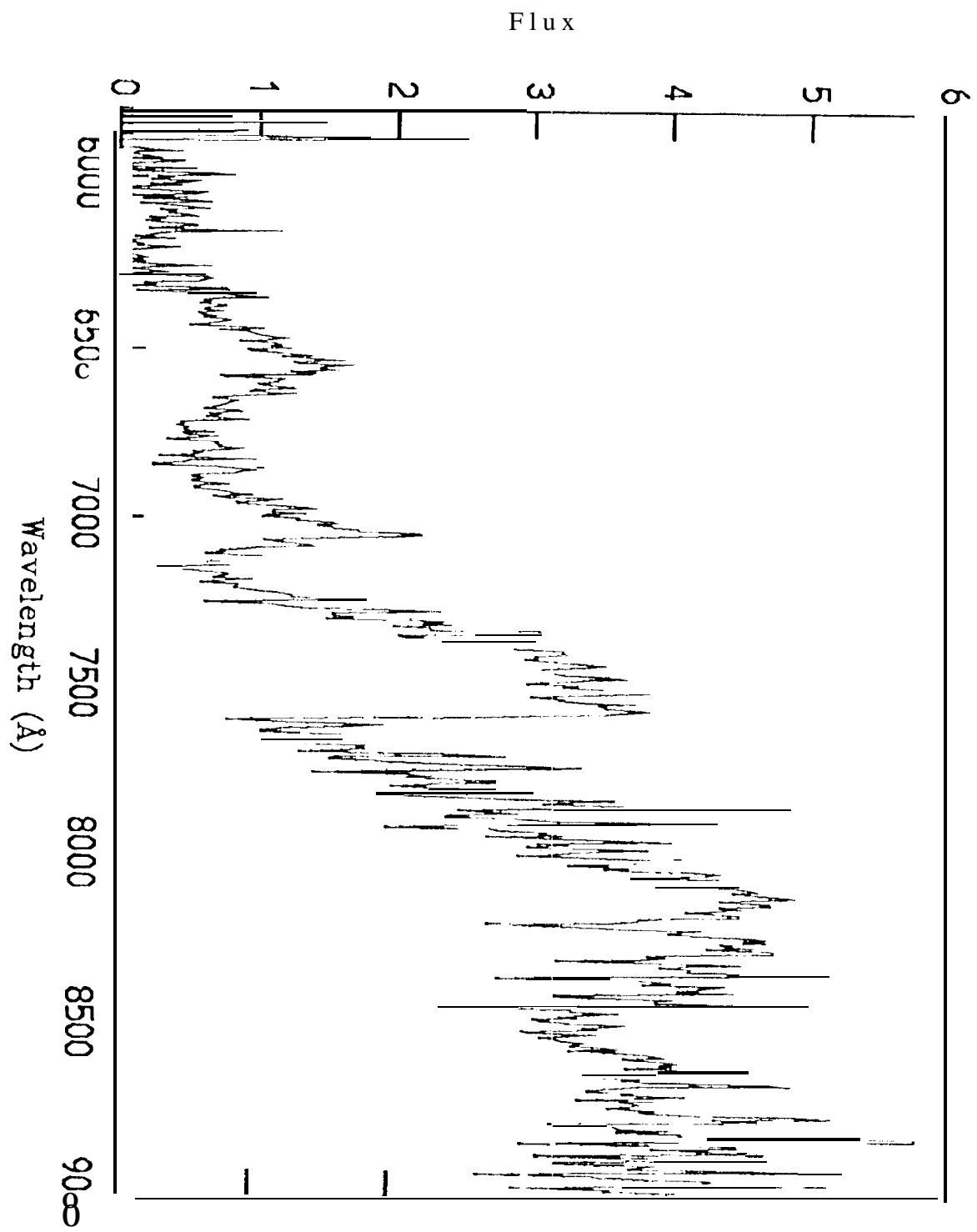


Fig 11

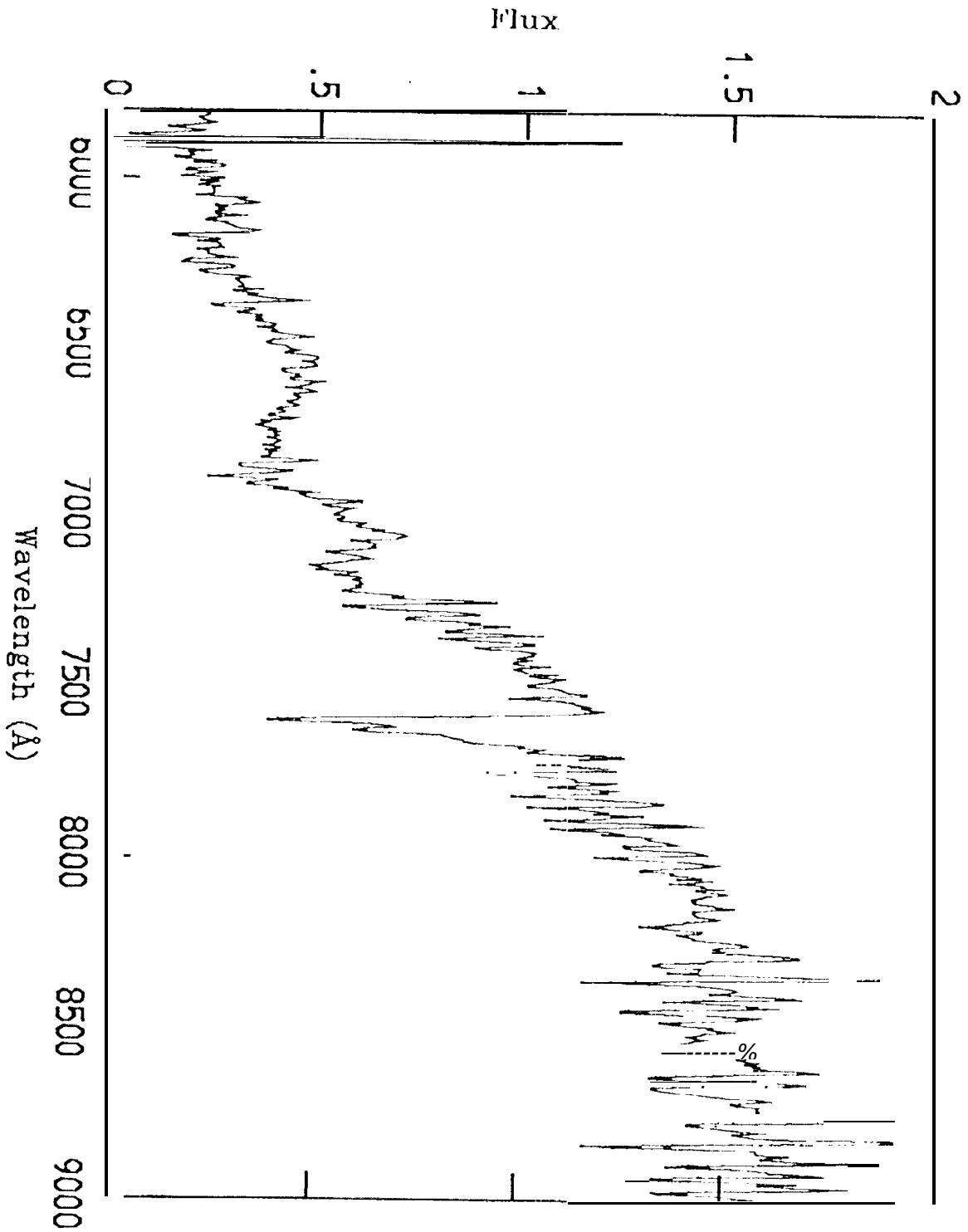


Fig 12

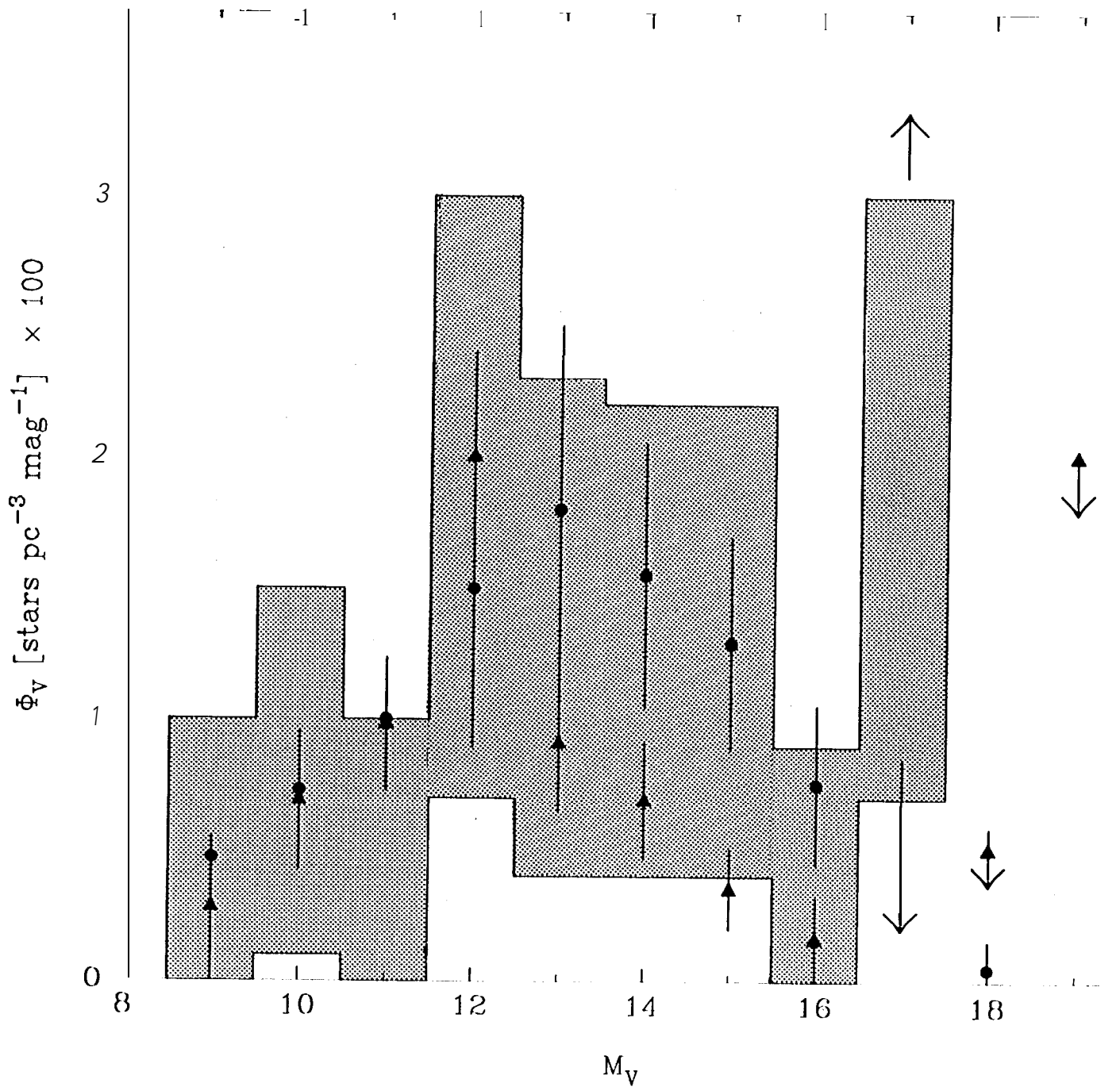


Fig 13

References

- Arc, J., & Greenstein, J.I. 1980, ApJ, 240, 859.
- Andre, P., Montmerle, T., & Feigelson, E.D. 1987, AJ, 93, 1182.
- Bahcall, J.N. and Soncira, R.M. 1980, ApJS, 44, 73.
- Beckert, D.C., & Newberry, M.V. 1989, PASP, 101, 849.
- Beichman, C.A., Myers, P.C., Emerson, J.P., Harris, S., Mathieu, R., Benson, P. J., & Jennings, R.E. 1986, ApJ, 307, 337.
- Beichman, C. A., Boulanger, F., & Moshir, M. 1991, IPAC Preprint No. 0076.
- Bessell, M.S. 1986, PASP, 98, 1303.
- Bessell, M.S. 1990, A&AS, 83, 357.
- Bessell, M.S. 1991, AJ, 101, 662.
- Bessell, M. S., & Weis, E.W. 1987, I'ASJ', 99, 642.
- Boeshaar, P. C., & Tyson, J.A. 1985, AJ, 90, 817.
- Bok, B.J. 1956, AJ, 61, 309.
- Bowen, I., S. 1960, in *Stars and Stellar Systems*, 1, ed. G.P. Kuiper, & B.M. Middlehurst (Chicago: University of Chicago Press), p. 43.
- Bruzual, G.A. 1966, Ph.D. Thesis, University of California, Berkeley.
- Cernicharo, J., & Guélin, M. 1987, A&A, 176, 299.
- Cousins, A.W.J. 1976, MmRAS, 81, 25.
- Cousins, A.W.J. 1980, S. African Astr. Obs. Circ., 1, 166.
- Dahn, C.C., Liebert, J., & Harrington, I.-? S. 1986, AJ, 91, 621.
- de Geus, Eugene 1988, Ph.D. Thesis, University of Leiden.
- Dickman, R.L. 1978, AJ, 83, 363.
- Dickman, R.L., & Herbst, W. 1990, ApJ, 357, 531.
- Elias, J.H. 1978a, ApJ, 224, 453.

- Elias, J.]. 1978b, ApJ, 224, 857.
- Feigelson, E.D. 1987, in *Protostars and Molecular Clouds*, cd. T. Montmerle, & C. Bertout (Saclay: CEA), p.123.
- Fernie, J.D. 1983, *Publ. Astron. Soc. Pac.*, **95**, 782.
- Fischer, D. A., & Marcy, G. 1992, ApJ, 396, 178.
- Gilmore, G. & Reid, N. 1983, MNRAS, 202, 1025.
- Hanson, R.B. 1983, in *The Nearby Stars and the Stellar Luminosity Function*, cd. A.G. Davis Philip & A.I.?, Uppgren (Schenectady: i. Davis Press), p. 51.
- Hawkins, M.R.S., & Bessell, M.S. 1988, MNRAS, 234, 177.
- Henry, T. J., & McCarthy, D.W. 1990, ApJ, 350, 334.
- Herbst, W., & Dickman, R. L. 1983, in *The Nearby Stars and the Stellar Luminosity Function*, cd. A.G. Davis Philip & A.R. Uppgren (Schenectady: L. Davis Press), p. 187.
- Ichikawa, T., & Nishida, M. 1989, AJ, 97, 1074
- Jarrett, T. 1992, Ph.D. Thesis, University of Massachusetts.
- Jarrett, T., Dickman, R. L., & Herbst, W. 1989, ApJ, 345, 881.
- Johnson, H.L., Mitchell, R.L., Iriarte, B., & Wisniewski, W. Z. 1966, *Comm. Lunar and Planetary Lab.*, 4, 99.
- Jones, B.F. & Herbig, G.H. 1979, AJ, 84, 18-2.
- Kirkpatrick, J.D., Henry, T.J., & McCarthy, D. 1991, ApJS, 77, 417
- Kron, R.G. 1980, ApJS, 43, 305.
- Landolt, Arlo 1983, AJ, 88, 439.
- Larson, R. II. 1986, MNRAS, 218, 409.
- Larson, R.B. 1992, MNRAS, 256, 641
- Leggett, S. K., & Hawkins, M.R.S. 1988, MNRAS, 234, 1065.
- Luyten, W. J. 1963, *Proper Motion Survey with the 48-Inch Schmidt Telescope* (Minneapolis: University of Minnesota), No. 1.
- Luyten, W.J. 1976, *Proper Motion Survey with the 48-Inch Schmidt Telescope* (Minneapolis: University of Minnesota), No. 46.

- McCuskey, S.W. 1969, *AJ*, 74, 807
- Mihalas, D., & Binney, J. 1981, *Galactic Astronomy* (San Francisco: W,11, Freeman & Company).
- Minkowski, R.L., & Abell, G.O. 1963, in *Stars and Stellar Systems*, 111, ed. G.P. Kuiper & B.M. Middlehurst (Chicago: University of Chicago Press), p. 481.
- Montmerle, T., Koch-Miramond, I., Falgarone, E., & Grindley, J.E. 1983, *ApJ*, 269, 182.
- Mundy, L.E., Wilking, B. A., & Myers, S. '1'. 1986, *ApJ*, 311, 175.
- Myers, P.C., Linke, R. A., & Benson, P.J. 1983, *ApJ*, 264, 517.
- Rana, N.C. 1987, *A&A*, 184, 104.
- Reid, N, 1987, *MNRAS*, 225, 873.
- Reid, N. 1991, *AJ*, 102, 1428.
- Reid, N., & Gilmore, G. 1982, *MNRAS*, 201, 73.
- Salpeter, E.E. 1955, *ApJ*, 121, 161.
- Savage, B.D., & Mathis, J.S. 1979, *ARA&A*, 17, 73.
- Scale, J.M. 1988, in *Starbursts and Galaxy Evolution*, ed. 'T'. Montmerle (Paris: Editions Frontieres).
- Schmidt, M. 1975, *ApJ*, 202, 22.
- Shu, F.H., Adams, F.C., & Lizano, S. 1987, *ARA&A*, 25, 23.
- Skrutskie, M. ii. 1987, Ph.D. Thesis, Cornell University.
- Skrutskie, M.F., Forrest, W. J., & Shure, M. 1989, *AJ*, 98, 1409.
- Stine, P.C., Feigelson, E.D., Andre, P., & Montmerle, "1". 1988, *AJ*, 96, 1394.
- Stobie, 1{ S., Ishida, K., & Peacock, J.A. 1989, *MNRAS*, 238, 709.
- Taylor, B.J. 1986, *ApJS*, 60, 577.
- Tinney, C.G., Mould, J.R., & Reid, I.N. 1992, *ApJ*, 396, 173.
- Walker, C. K., Lada, C.J., Young, E., Maloney, P. R., & Wilking, B.A. 1986, *ApJ*, 309, 1.47.
- Wielen, R., Jahreis, H., & Krueger, R. 1983, in *The Nearby Stars and the Stellar Luminosity Function*, ed. A.(i. Davis Philip & A.R. Upgren (Schenectady: L. Davis Press), p. 163.
- Wilking, B. A., & Lada, C.J. 1983, *ApJ*, 274, 698.